Magnesium, ADP, and Actin Binding Linkage of Myosin V: Evidence for Multiple Myosin V−ADP and Actomyosin V−ADP States†

Diane E. Hannemann,‡ Wenxiang Cao,‡ Adrian O. Olivares, James P. Robblee, and Enrique M. De La Cruz*

Department of Molecular Biophysics and Biochemistry, Yale University, 260 Whitney Avenue, New Haven, Connecticut 06520

Received December 16, 2004; Revised Manuscript Received April 28, 2005

ABSTRACT: The [Mg^{2+}] dependence of ADP binding to myosin V and actomyosin V was measured from the fluorescence of mantADP. Time courses of MgmantADP dissociation from myosin V and actomyosin V are biphasic with fast observed rate constants that depend on the [Mg^{2+}] and slow observed rate constants that are [Mg^{2+}]-independent. Two myosin V−MgADP states that are in reversible equilibrium, one that exchanges nucleotide and cation slowly (strong binding) and one that exchanges nucleotide and cation rapidly (weak binding), account for the data. The two myosin V−MgADP states are of comparable energies, as indicated by the relatively equimolar partitioning at saturating magnesium. Actin binding lowers the affinity for bound Mg^{2+} 2-fold but shifts the isomerization equilibrium ~6-fold to the weak ADP binding state, lowering the affinity and accelerating the overall rate of MgADP release. Actin does not weaken the affinity or accelerate the release of cation-free ADP, indicating that actin and ADP binding linkage is magnesium-dependent. Myosin V and myosin V−ADP binding to actin was assayed from the quenching of pyrene actin fluorescence. Time courses of myosin V−ADP binding and release are biphasic, consistent with the existence of two (weak and strong) quenched pyrene actomyosin V−ADP conformations. We favor a sequential mechanism for actomyosin V dissociation with a transition from strong to weak actin-binding conformations preceding dissociation. The data provide evidence for multiple myosin−ADP and actomyosin−ADP states and establish a kinetic and thermodynamic framework for defining the magnesium-dependent coupling between the actin and nucleotide binding sites of myosin.

The myosin family of molecular motors constitutes a large gene family of proteins that transport biological molecules along actin filament tracks and have been implicated in various cellular functions including membrane trafficking, cytokinesis, cell migration, and signal transduction (*1*). At least 18 different classes (classes I−XVIII) make up the family. All identified myosins possess a highly conserved catalytic motor domain that binds actin, hydrolyzes ATP, and performs the mechanical work.

The actomyosin ATPase cycle consists of a series of nucleotide-linked, biochemical reactions that are coupled to energetic and conformational changes in myosin (*2*). Myosin without bound nucleotide binds actin filaments with high affinity. ATP binding opens the actin-binding cleft of myosin, which lowers its affinity for actin, causing myosin to dissociate from actin. Detached myosin undergoes a conformational change that allows it to hydrolyze ATP to ADP and P_i. The hydrolysis products remain bound noncovalently to myosin, yielding the kinetically stable but thermodynamically unstable high-energy myosin−ADP−P_i intermediate. Myosin−ADP−P_i binding to actin accelerates rate-limiting P_i release. This transition increases the affinity of myosin for actin and accompanies the force-generating power stroke. ADP release generates actomyosin with no bound nucleotide, and the catalytic cycle begins again with ATP binding.

Understanding the linkage between actin binding and the chemical state of the bound nucleotide is a central issue in defining the mechanism of force generation and work output by myosin motors. Actin binding weakens the affinity and accelerates the release of the hydrolysis products, ADP and P_i, from myosin. In this regard actin can be considered a nucleotide exchange factor for myosin (*3*) similar to the regulatory proteins that act on members of the G-protein family. In this system, binding of the exchange factor disrupts the coordination of the nucleotide-associated cation, which accelerates the overall release of the bound nucleotide (*4*). This mechanistic strategy has also been reported for other nucleotide exchange proteins such as profilin, which accelerates nucleotide exchange from actin monomers (*5*), and kinesin, where microtubule binding accelerates the release of MgADP (*6*). It is clear that, for many proteins, coordination of the nucleotide-associated cation frequently plays an important role in regulating the nucleotide binding affinities and kinetics of release.

Myosin V is a processive two-headed myosin that takes multiple steps along actin before dissociating. It accomplishes this task, in part, by spending the majority of its ATPase cycle time strongly bound to actin and ADP so that ADP release is the rate-limiting step (*7*). Compared to other myosins, the coupling between actin and ADP binding is weak for myosin V and actin binding has minimal effects

† This work was supported by grants from the American Heart Association (No. 0235203N) and the National Science Foundation (MCB-0216834) to E.M.D.L.C. W.C. is supported by an Anderson endowed postdoctoral fellowship from Yale University. A.O.O. is supported by an NIH predoctoral fellowship (No. 1F31AR051614-01).

* To whom correspondence should be addressed. Tel: (203) 432-5424. Fax: (203) 432-1296. E-mail: enrique.delacruz@yale.edu.

‡ Authors contributed equally to this work.

10.1021/bi0473509 CCC: $30.25
Published on Web 05/27/2005

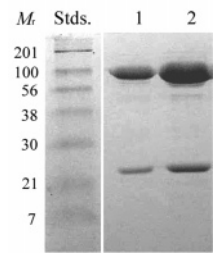

FIGURE 1: SDS−PAGE gel of recombinant myosin V-1IQ. 12% SDS−PAGE analysis of purified myosin V-1IQ (lanes 1 and 2) at two different loading densities. Note the absence of actin contamination.

on the affinity of myosin V for ADP (*7*), enabling it to simultaneously bind both actin and ADP with high affinity.

We initiated this study to determine the role of bound magnesium in dictating the ADP and actin affinities of myosin V and to evaluate if the coupling between actin and ADP binding to myosin V is [Mg^{2+}]-dependent. Our results establish a kinetic and thermodynamic framework for defining the magnesium-dependent coupling between the actin and nucleotide binding sites of myosin, and demonstrate that actin weakens ADP binding to myosin V by disrupting coordination of bound Mg^{2+} and shifting the equilibrium between two myosin V−ADP states to favor formation of the state that binds nucleotide and cation weakly.

EXPERIMENTAL PROCEDURES

Reagents. ADP (Sigma A-5285, purity 99+% as assayed by HPLC, data not shown) was purchased from Sigma (St. Louis, MO). ADP concentrations were determined by absorbance at 259 nm using ϵ_{259} of 15 400 M^{-1} cm^{-1}. *N*-Methylanthraniloyl-ADP (mantADP,[1] mixed 2′ and 3′ isomers) was purchased from Molecular Probes (Eugene, OR; Catalog No. M-12416, Lot No. 12B1-3); 2′-deoxy-mantADP was synthesized as described (*8*). MantADP concentrations were determined using ϵ_{255} of 23 300 M^{-1} cm^{-1}. $MgCl_2$ solution (1 M) was purchased from American Bioanalytical.

Protein Expression and Purification. Single-headed chicken myosin V-1IQ with bound light chain 1sa (referred to as myosin V throughout) was purified from Sf9 cells by Flag affinity chromatography (*7, 9*). Purity was >98% for all preparations (Figure 1). Actin was purified from rabbit skeletal muscle and gel filtered over Sephacryl S-300HR. Ca^{2+}-actin monomers were converted to Mg^{2+}-actin monomers with 0.2 mM EGTA and 50 μM (excess over actin) $MgCl_2$ immediately prior to polymerization by dialysis into KMg50 buffer (50 mM KCl, 1 mM EGTA, 1 mM DTT, 2 mM $MgCl_2$ and 10 mM imidazole, pH 7.0). Phalloidin (1.1 molar equiv) was used to stabilize actin filaments.

Stopped-Flow Measurements. All experiments were performed in K50 buffer (50 mM KCl, 1 mM EGTA, 1 mM DTT, and 10 mM imidazole, pH 7.0) supplemented with varying concentrations of $MgCl_2$ using an Applied Photophysics (Surrey, U.K.) SX.18MV-R stopped flow apparatus thermostated at 25 (±0.1) °C. The free [Mg^{2+}] in solution (i.e. not bound to nucleotides or myosin) was calculated using the affinities of Mg^{2+} for ADP, as determined by isothermal titration calorimetry, and EDTA under our experimental conditions. Essentially identical values were obtained using the program MaxC 2.5 (http://www.stanford.edu/~cpatton/).

Time courses of fluorescence change were fitted to a sum of exponentials (eq 1) by nonlinear least-squares fitting using Pro-K software provided with the instrument:

$$F(t) = F_\infty + \sum_{i=1}^{n} A_i \, e^{-k_i t} \quad (1)$$

where $F(t)$ is the fluorescence at time t, F_∞ is the final fluorescence intensity, A_i is the amplitude, k_i is the observed rate constant characterizing the ith relaxation process, and n is the total number of observed relaxations. The dead time of the instrument determined from the reduction of 2,6-dichlorophenolindophenol in absorbance mode is <2 ms. Fitting was limited to data beyond 3 ms to account for instrument dead time and to exclude data acquired during the continuous flow phase of mixing as recommended by the manufacturer. Time courses shown are of unaveraged, 1000-point transients collected with the instrument in oversampling mode (intrinsic time constant ~30 μs) or, where indicated, the average of two individual traces. In most cases the average of 3−6 transients was used for analysis. Uncertainties are reported as standard errors in the fits unless stated otherwise.

MantADP Dissociation Kinetics. MantADP release was measured by competing an equilibrated sample of myosin−mantADP or actomyosin−mantADP (in the presence of 4 mM EDTA or 0.2 mM $MgCl_2$) with >100-fold excess unlabeled ADP (in the presence of 4 mM EDTA or a range of [$MgCl_2$]). Excess unlabeled ADP ensures that mantADP dissociation is irreversible. Fluorescence (λ_{ex} = 297 nm) was monitored through a 400 nm long pass colored glass filter.

MantADP release from actomyosin V−ADP−P_i (and actomyosin V−ADP) was measured with the instrument in sequential mixing mode: 2 μM myosin V was mixed with 100 μM mantADP or mantATP (mixture of 2′ and 3′), aged for ~2 s to allow for product (ADP−P_i or the strong ADP binding state) formation, and then mixed with 60 μM actin filaments and 4 mM MgADP. Final concentrations are 0.67 μM myosin V, 33 μM mantADP or mantATP, 30 μM F-actin, and 2 mM MgADP.

MantADP Binding Kinetics. Time courses of mantADP binding were acquired under pseudo-first-order conditions with [nucleotide] ≫ [myosin or actomyosin]. Actomyosin samples were prepared by mixing myosin with 4 μM actin filaments and equilibrating at 25 °C for at least 10 min. Samples were treated with apyrase (potato, grade VII, 0.1 unit mL^{-1} final) to ensure rigor (no nucleotide) conditions.

Actin Binding and Dissociation Kinetics. Myosin V and myosin V−ADP binding to actin filaments was monitored by fluorescence quenching of pyrene actin. Fluorescence (λ_{ex} = 366 nm) was monitored through a 400 nm long pass colored glass filter. Myosin V and myosin V−ADP binding to actin filaments was measured under pseudo-first-order conditions with [actin] ≫ [myosin]. Myosin V and myosin V−ADP dissociation from pyrene actin filaments was monitored by mixing an equilibrated mixture of pyrene

[1] Abbreviations: mantADP or mD, 2′(or 3′)-*O*-(*N*-methylanthraniloyl) adenosine 5′-diphosphate; MgmantADP, magnesium in complex with mantADP; S1, fast skeletal muscle myosin subfragment-1; actoS1.ADP, S1 in complex with actin and ADP.

actomyosin V with >40-fold excess unlabeled actin filaments. Mg^{2+}-free and saturating Mg^{2+} conditions were obtained by the addition of 4 mM EDTA or 5 mM $MgCl_2$, respectively, to K50 buffer. Nucleotide-free conditions were achieved by incubating myosin V with apyrase (0.1 unit mL^{-1}) at 25 °C for 20 min. Time courses were corrected for photobleaching by subtracting the time courses of pyrene actin fluorescence acquired under identical experimental conditions.

Isothermal Titration Calorimetry. The affinity of Mg^{2+} for ADP was measured at 25 (±0.1) °C in K50 buffer essentially as described (*10, 11*) with a MicroCal (Northampton, MA) MCS isothermal titration calorimeter. DTT was not included in the reaction buffer to eliminate DTT related baseline problems. Data analysis was done with Origin software accompanying the instrument.

RESULTS

A. [Mg^{2+}] Dependence of MantADP Dissociation from Myosin V. MantADP dissociation from myosin V was measured by competition with unlabeled ADP. In the presence of 3 mM free Mg^{2+}, the time course of fluorescence change after mixing myosin V−mantADP (mixed 2′ and 3′ isomers) with excess MgADP follows a double exponential (Figure 2A) with fast (10.8 ± 0.9 s^{-1}) and slow (2.2 ± 0.1 s^{-1}) observed rate constants. The time course of 2′-deoxy-mantADP dissociation from myosin V also follows a double exponential (Figure 2C) with fast (13.3 ± 0.5 s^{-1}) and slow (2.3 ± 0.1 s^{-1}) observed rate constants comparable to those of the mixed isomers, confirming that the biphasic time courses are not due to the mixed 2′- and 3′-labeled isomers. The relative amplitude of the fast and slow phases for both mantADP and 2′-deoxy-mantADP are 30% and 70%, respectively. The time course of mantADP release when mixing with excess MgATP is also biphasic with a fast observed rate constant of 12.0 ± 0.1 s^{-1} and slow observed rate constant of 2.0 ± 0.03 s^{-1} (data not shown). This indicates that the ADP biphasic dissociation from myosin V is independent of the competing unlabeled ligands.

The observed rate constant of the fast dissociation depends strongly on the magnesium concentration and is saturated at ~2 mM free Mg^{2+} (Figure 3A). The slow phase is weakly dependent on magnesium concentration (Figure 3B).

The time course of mantADP release from myosin V in the presence of excess EDTA and no added magnesium (free [Mg^{2+}] ~ 0) can be well-fitted to a single exponential with an observed rate constant of 47.3 ± 1.3 s^{-1} (Figure 2A), indicating that divalent cation-free ADP dissociates from myosin V ~5 times more rapidly than MgADP (k_{-mD} > $k_{-Mg,mD}$ in Scheme 1).

The time course of mantADP release from myosin V after mixing an equilibrated mixture of myosin V−mantADP and 0.2 mM magnesium with excess EDTA (which leaves ~100 nM free Mg^{2+} in solution after mixing) deviates slightly from a single exponential (data not shown), with a fast observed rate constant of 44.0 ± 1.3 s^{-1} and a small slow phase amplitude comprising ~4.5% of the total amplitude. Since the rate of ADP dissociation measured by mixing myosin V−MgADP with excess EDTA is essentially identical to dissociation from myosin V−ADP in the absence of Mg^{2+}, bound Mg^{2+} must dissociate from myosin V−MgADP more rapidly than cation-free ADP dissociates (i.e. Mg^{2+} dissociates from myosin−MgADP at >47 s^{-1} and ADP release is not limited by Mg^{2+} dissociation). EDTA makes Mg^{2+} dissociation irreversible, and ADP is released as a divalent cation-free species. If bound Mg^{2+} dissociated only as a complex with ADP, EDTA would bind Mg^{2+} after MgADP release and would not accelerate the observed mantADP dissociation rate constant.

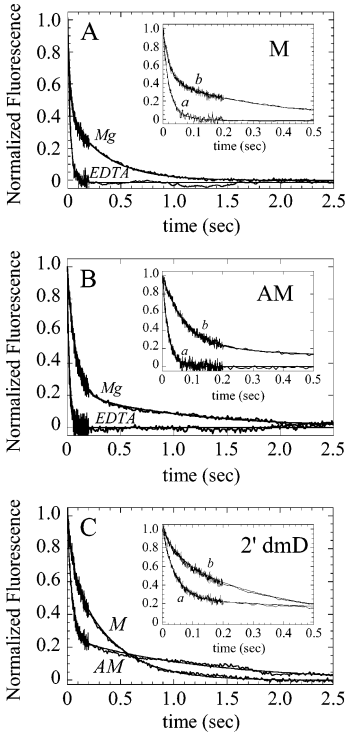

FIGURE 2: Kinetics of MantADP dissociation from myosin V and actomyosin V. (A) Time courses of fluorescence change upon mixing an equilibrated mixture of 20 μM mantADP and 0.8 μM myosin V with an equal volume of (curve *EDTA*) 4 mM ADP with final conditions after mixing of 4 mM EDTA, or (curve *Mg*) 4 mM MgADP with final conditions after mixing of 3 mM free Mg^{2+}. Data was collected on a split time base with fewer data points after 200 ms, accounting for the reduced noise level. Inset: Time courses shown on a shorter time scale. The smooth lines through the data represent best fits to single (curve *a* = *EDTA*, rate constant: 47.3 s^{-1}) or double (curve *b* = *Mg*, rate constant: 10.8 (30%) and 2.2 s^{-1} (70%)) exponentials. The data traces represent the averages of two individual transients. (B) Time courses of fluorescence change after mixing an equilibrated mixture of 20 μM mantADP and 0.8 μM actomyosin V with an equal volume of (curve *EDTA*) 4 mM ADP with final conditions after mixing of 4 mM EDTA, or (curve *Mg*, rate constant: 13.8 s^{-1} (80%) and 1.0 s^{-1} (20%)) 4 mM MgADP with final conditions after mixing of 3 mM free Mg^{2+}. The data traces represent individual unaveraged transients. The smooth lines through the data represent best fits to single (curve *EDTA*, rate constant: 44.7 s^{-1}) or double (curve *Mg*) exponentials. Inset: Time courses shown on a shorter time scale. (C) Time courses of fluorescence decrease upon mixing an equilibrated mixture of 20 μM 2′-deoxy mantADP and (curve *AM*) 0.8 μM actomyosin V or (curve *M*) 0.8 μM myosin V with an equal volume of 4 mM MgADP with final conditions of 3 mM free Mg^{2+}. Inset: Same data plotted on a shorter time scale. The smooth lines through the data represent best fits to double exponentials. The data traces represent the average of two individual transients.

We interpret the biphasic time courses of mantADP release in the presence of magnesium, the [Mg^{2+}] dependence of the observed fast dissociation rate constant, and the weak [Mg^{2+}] dependence of the observed slow dissociation rate constant to mean that there are two myosin V−ADP states,

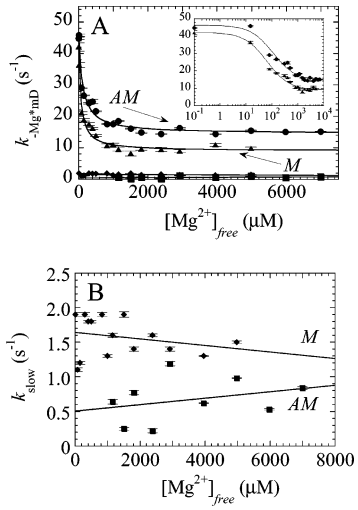

FIGURE 3: $[Mg^{2+}]$ dependence of mantADP dissociation from myosin V and actomyosin V. (A) $[Mg^{2+}]$ dependence of the observed rate constants of mantADP dissociation from myosin V (fast, ▲; slow, ◆) and actomyosin V (fast, ●; slow, ■). Solid lines through the data represent the best fits to eq 5. (B) $[Mg^{2+}]$ dependence of the slow observed rate constants of mantADP dissociation from myosin V (◆) and actomyosin V (■). The solid lines represent the best fits to a straight line.

Scheme 1

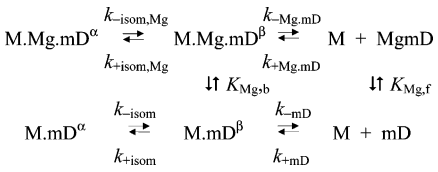

one that readily exchanges cation with solution (M.Mg.mD$^{\beta}$) and one that does not (M.Mg.mD$^{\alpha}$), and favor the reaction mechanism in Scheme 1 to describe the mechanism of ADP and Mg^{2+} exchange from myosin V. In Scheme 1, M is myosin V, Mg is the divalent magnesium cation, Mg.mD is the Mg^{2+}−ADP complex, and mD is cation-free mantADP. Scheme 1 ignores formation of a collision complex which is likely to be an intermediate preceding formation of the β states along the nucleotide binding pathway. The top pathway in Scheme 1 represents ADP dissociation in the presence of saturating Mg^{2+}, and the bottom pathway represents ADP dissociation in the absence of Mg^{2+}. The fast phase of mantADP dissociation, in the presence of magnesium, represents dissociation through both $k_{-Mg.mD}$ (with saturating Mg^{2+}) and k_{-mD} (without Mg^{2+}) pathways. EDTA chelates Mg^{2+} and favors flux through k_{-mD} (Scheme 1).

The single phase of ADP dissociation observed in the absence of added Mg^{2+} and in the presence of excess EDTA indicates that the M.mD$^{\alpha}$ state (Scheme 1) is not significantly (≤10%) populated when Mg^{2+} is absent. Therefore, the observed rate constant of the slow phase (k_{slow}) in the presence of saturating Mg^{2+} represents contributions from isomerization of M.Mg.mD$^{\alpha}$ to M.Mg.mD$^{\beta}$ ($k_{+isom,Mg}$ and $k_{-isom,Mg}$).

At any given Mg^{2+} concentration, the effective rate constants $k_{-Mg*.mD}$, $k_{+isom,Mg*}$, and $k_{-isom,Mg*}$ (the symbol * denotes any given $[Mg^{2+}]$ to distinguish from $k_{-Mg.mD}$ and $k_{+isom,Mg}$, the fundamental rate constants at saturating $[Mg^{2+}]$), can be calculated from the fast (k_{fast}) and slow (k_{slow}) observed rate constants and the fast phase amplitude (A_{fast}) according to the following (see Appendix):

Table 1: Summary of the Rate and Equilibrium Constants Outlined in Scheme 1

ADP and MgADP Binding		Mg^{2+} Binding	
K_{mD} (μM)	4.6	$K_{Mg,b}$ (μM)	65 ± 11
k_{+mD} (μM^{-1} s^{-1})	9.2 ± 0.2	$K_{Mg,f}$ (μM)	350 ± 30
k_{-mD} (s^{-1})	44.0 ± 1.3[a]		
	47.3 ± 1.3[c]	ADP Isomerization	
	42.0 ± 1.4[d]	K_{isom}	≥10
	46.3 ± 2.3[e]	$K_{isom,Mg}$	0.59
$K_{Mg.mD}$ (μM)	1.8	$k_{+isom,Mg}$ (s^{-1})	3.4
$k_{+Mg.mD}$ (μM^{-1} s^{-1})	4.9 ± 0.2[b]	$k_{-isom,Mg}$ (s^{-1})	2.0
$k_{-Mg.mD}$ (s^{-1})	10.8 ± 0.9[b]		
	9.0 ± 0.6[d]	$K_{Mg.mD,overall}$ (μM)	0.67

[a] Measured by competing myosin−Mg^{2+}−mantADP with 4 mM EDTA. [b] Measured in the presence of saturating (≥2 mM) Mg^{2+}. [c] Measured in the presence no added Mg^{2+} and in the presence of EDTA. [d] Estimated from the best fit (Figure 3A). [e] Estimated from the *y*-intercept of the best fit (Figure 5A).

$$k_{fast} = k_{-Mg*.mD} + k_{+isom,Mg*} \quad (2)$$

$$k_{slow} = k_{-isom,Mg*}\left(\frac{k_{-Mg*.mD}}{k_{-Mg*.mD} + k_{+isom,Mg*}}\right) \quad (3)$$

$$A_{fast} = \left(\frac{k_{-isom,Mg*}}{k_{+isom,Mg*} + k_{-isom,Mg*}}\right)\left(\frac{k_{-Mg*.mD}}{k_{-Mg*.mD} + k_{+isom,Mg*}}\right) \quad (4)$$

The isomerization rate constants $k_{+isom,Mg}$ and $k_{-isom,Mg*}$ were calculated by averaging $k_{+isom,Mg*}$ and $k_{-isom,Mg*}$ (calculated using eqs 2, 3, and 4) values at saturating (≥2 mM) Mg^{2+} (Figure 3, Table 1) and were used to calculate the isomerization equilibrium constant ($K_{isom,Mg} = k_{-isom,Mg*}/k_{+isom,Mg}$) in the presence of saturating (≥2 mM free) Mg^{2+}. The value of 0.59 for $K_{isom,Mg}$ (Table 1) indicates that the equilibrium between the two myosin V−ADP binding states (M.Mg.mD$^{\alpha}$ and M.Mg.mD$^{\beta}$) favors formation of the strong ADP binding state (M.Mg.mD$^{\alpha}$).

MantADP dissociates as a cation-free species with rate constant k_{-mD} in the absence of cation, and as a metal−nucleotide complex with rate constant $k_{-Mg.mD}$ in the presence of saturating Mg^{2+}. At intermediate Mg^{2+} concentrations, dissociation through both pathways ($k_{-Mg.mD}$ and k_{-mD}) contributes to the effective mantADP dissociation rate constant ($k_{-Mg*.mD}$) which can be expressed in terms of $k_{-Mg.mD}$ and k_{-mD} as (see Appendix)

$$k_{-Mg*.mD} = \frac{k_{-Mg.mD}[Mg] + k_{-mD}K_{Mg,b}}{[Mg] + K_{Mg,b}} \quad (5)$$

where $K_{Mg,b}$ is the dissociation equilibrium constant for Mg^{2+} binding to myosin V with bound mantADP (M.Mg.mD$^{\beta}$).

The $[Mg^{2+}]$ dependence of the dissociation rate constant $k_{-Mg*.mD}$ was calculated using eqs 2, 3, and 4 (Figure 3A). The best fit of the $[Mg^{2+}]$ dependence of $k_{-Mg*.mD}$ to eq 5 yields an affinity ($K_{Mg,b}$) of 65 ± 11 μM for Mg^{2+} binding to myosin V−mantADP (Figure 3A). Extrapolation of the data to the limit of $[Mg^{2+}] = 0$ yields a rate constant (k_{-mD}) of 42.0 ± 1.4 s^{-1} for divalent cation-free mantADP dissociation from myosin V, comparable to the rate measured directly by mixing with excess EDTA and no added Mg^{2+}

Scheme 2

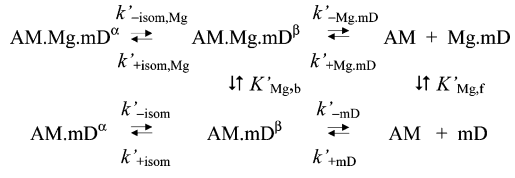

(47.3 ± 1.3 s^{-1}, Figure 2A). Extrapolation of the data to [Mg] = ∞ indicates that Mg^{2+}−mantADP dissociates more slowly with a rate constant ($k_{-Mg.mD}$) of 9.0 ± 0.6 s^{-1} (Figure 3A). The rate and equilibrium constants of Scheme 1 are summarized in Table 1.

B. [Mg^{2+}] Dependence of mantADP Dissociation from Actomyosin V. In the presence of 3 mM free Mg^{2+} the time course of fluorescence change after mixing actomyosin V−mantADP with excess MgADP follows a double exponential (Figure 2B) with fast (13.8 ± 0.2 s^{-1}, 80%) and slow (1.0 ± 0.1 s^{-1}, 20%) observed rate constants. As with myosin V in the absence of actin, the fast observed rate constants depend strongly on [Mg^{2+}] and saturate at ∼2 mM free Mg^{2+} (Figure 3A) and the slow phases depend weakly on [Mg^{2+}] (Figure 3B). The time course of 2′-deoxy-mantADP dissociation from actomyosin V also follows a double exponential (Figure 2C) with fast (24.0 ± 0.3 s^{-1}) and slow (0.8 ± 0.1 s^{-1}) observed rate constants. The slow phase was smaller when ATP was used to displace bound mantADP (data not shown).

The time course of mantADP release from actomyosin V in the presence of excess EDTA and no added magnesium can be well-fitted to a single exponential with an observed rate constant of 44.7 ± 1.0 s^{-1} (Figure 2B), ∼3 times more rapid than with Mg^{2+}. In addition, the time course of mantADP release from actomyosin V after mixing an equilibrated mixture of actomyosin V−mantADP and 0.2 mM magnesium with excess EDTA (which leaves ∼100 nM free Mg^{2+} in solution after mixing) deviates slightly from a single exponential (data not shown), with a fast observed rate constant of 44.4 ± 0.4 s^{-1} and a slow observed rate constant of 1.2 ± 0.2 s^{-1} comprising ∼4−5% of the total amplitude.

We favor a similar reaction mechanism (Scheme 2) to describe the biphasic time courses of mantADP release from actomyosin V and the [Mg^{2+}] dependence of the mantADP dissociation rate constants. In Scheme 2, AM.Mg.mD$^{\beta}$ exchanges bound cation rapidly and AM.Mg.mD$^{\alpha}$ does not exchange cation as supported by the lack of [Mg^{2+}] dependence of the slow phase. Scheme 2 ignores formation of a collision complex which is an intermediate preceding formation of the β states along the binding pathway (*12*). The top and bottom pathways (Scheme 2) represent ADP dissociation in the presence of saturating Mg^{2+} and in the absence of Mg^{2+}, respectively. The single phase of ADP dissociation observed in the absence of added magnesium and excess EDTA indicates that the AM.mD′ state is not populated to a great extent (≤10%) without Mg^{2+}.

As described for myosin V in the absence of actin (Scheme 1), the rate constants, $k'_{-Mg^*.mD}$, k'_{+isom,Mg^*}, and k'_{-isom,Mg^*}, at any Mg^{2+} concentration can be determined from the observed fast and slow rate constants and the fast phase amplitude (eqs 2, 3, and 4). The best fit of the [Mg^{2+}] dependence of the rate constant ($k'_{-Mg^*.mD}$), reflecting ADP dissociation from the weak ADP binding state (AM.Mg.mD$^{\beta}$), to eq 5 (Figure 3A) yields an affinity ($K'_{Mg,b}$) of 110 ± 21 μM for Mg^{2+} binding to actomyosin V−mantADP (Figure 3A). Extrapolation of the data to the limit of [Mg^{2+}] = 0 yields a rate constant (k'_{-mD}) of 46.2 ± 1.5 s^{-1} for divalent cation-free mantADP dissociation from actomyosin V, comparable to the observed rate constant measured directly in the presence of excess EDTA and no added magnesium (44.7 ± 1.0 s^{-1}; Figure 2B). Mg^{2+}−mantADP dissociates from actomyosin V more slowly with a rate constant (k'_{-MgmD}) of 14.5 ± 0.7 s^{-1} (from the best fit), in agreement with published values determined under comparable conditions (*7*, *13*, *14*).

Table 2: Summary of the Rate and Equilibrium Constants Outlined in Scheme 2

ADP and MgADP Binding		Mg^{2+} Binding	
K'_{mD} (μM)	4.5	$K'_{Mg,b}$ (μM)	110 ± 21
k'_{+mD} (μM^{-1} s^{-1})	10.2 ± 0.7	$K_{Mg,f}$ (μM)	350 ± 30
k'_{-mD} (s^{-1})	44.4 ± 0.4[a]		
	44.7 ± 1.0[c]	ADP Isomerization	
	46.2 ± 1.5[d]	K'_{isom}	≥10
	39.7 ± 1.5[e]	$K'_{isom,Mg}$	3.8
$K'_{Mg.mD}$ (μM)	2.3	$k'_{+isom,Mg}$ (s^{-1})	0.18
$k'_{+Mg.mD}$ (μM^{-1} s^{-1})	6.2 ± 0.6[b]	$k'_{-isom,Mg}$ (s^{-1})	0.68
$k'_{-Mg.mD}$ (s^{-1})	13.8 ± 0.2[b]		
	14.5 ± 0.7[d]	$K'_{Mg.mD,overall}$ (μM)	1.8

[a] Measured by competing myosin−Mg^{2+}−mantADP with 4 mM EDTA. [b] Measured in the presence of saturating (≥2 mM) Mg^{2+}. [c] Measured in the presence no added Mg^{2+} and in the presence of EDTA. [d] Estimated from the best fit (Figure 3A). [e] Estimated from the *y*-intercept of the best fit (Figure 5A).

The fundamental isomerization rate constants, $k'_{+isom,Mg}$ and $k'_{-isom,Mg}$, were calculated by averaging the values of k'_{+isom,Mg^*} and k'_{-isom,Mg^*} at ≥2 mM free Mg^{2+}, and yield an isomerization equilibrium constant ($K'_{isom,Mg} = k'_{-isom,Mg}/k'_{+isom,Mg}$) of 3.8 (Table 2), indicating that the equilibrium between the two actomyosin ADP binding states (AM.Mg.mD$^{\alpha}$ and AM.Mg.mD$^{\beta}$) favors formation of the weak ADP binding state (AM.Mg.mD$^{\beta}$). This is in contrast to the myosin V−ADP complex, where the M.Mg.mD$^{\alpha}$ and M.Mg.mD$^{\beta}$ equilibrium favors strong ADP binding (M.Mg.mD$^{\alpha}$). Therefore, actin binding shifts the isomerization equilibrium to favor weak ADP binding.

C. MantADP Binding to Myosin V. Time courses of mantADP binding to myosin V in the presence of 2 mM Mg^{2+} or excess EDTA are biphasic (Figure 4A). Without magnesium, the slow phase is ≤10% of the overall signal, consistent with low population of the strong MgADP binding state. The fast observed rate constants depend linearly on the mantADP concentration ([MgmD]) over the range examined (Figure 5A, see eq A21 of Appendix),

$$k_{fast} = k_{+MgmD}[MgmD] + k_{-MgmD} \quad (6)$$

permitting the rate constants ($k_{+Mg.mD}$ and $k_{-Mg.mD}$) to be obtained from the slope and *y*-intercept of the linear fit of the mantADP concentration dependence of the observed fast rate (Figure 5A). In the presence of saturating magnesium, the second-order association rate constant obtained from the slope is 4.9 ± 0.2 μM^{-1} s^{-1} (Table 1), in agreement with the published values (*7*, *9*, *13*). The MgmantADP dissociation rate constant ($k_{-Mg.mD}$) estimated from the *y*-intercept is 3.5 ± 1.6 s^{-1} (Figure 5A). In the presence of saturating magnesium, the observed rate constants of the slow phases

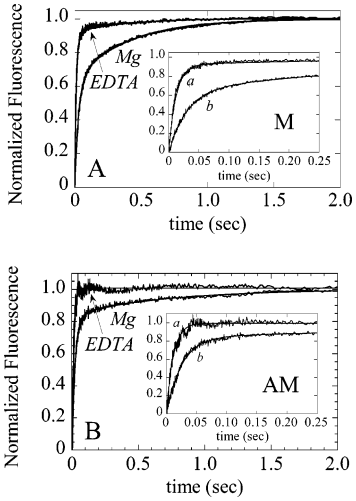

FIGURE 4: Kinetics of mantADP binding to myosin V and actomyosin V. A. Time courses of fluorescence enhancement after mixing 0.4 μM myosin V with 6.4 μM mantADP (final concentrations) in 2 mM EDTA (curve *EDTA*) or 3 mM Mg^{2+} (curve *Mg*). The data are of individual unaveraged transients. The smooth lines through the data represent the best fits to double exponentials. Inset: Same data plotted on a shorter time scale. (B) Time courses of fluorescence enhancement after mixing 0.4 μM actomyosin V with 6.4 μM mantADP (final concentrations) in 2 mM EDTA (curve *EDTA*) or 3 mM Mg^{2+} (curve *Mg*). The data traces represent individual unaveraged transients. The smooth lines through the data represent the best fits to double exponentials. Inset: Same data plotted on a shorter time scale.

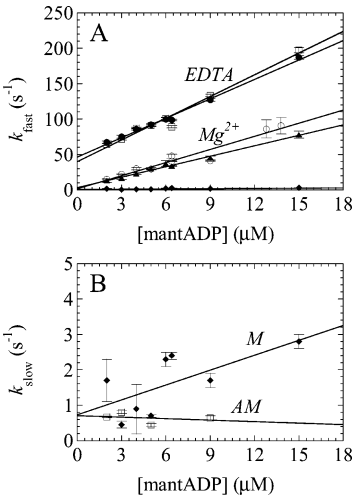

FIGURE 5: Concentration dependence of mantADP binding to myosin V and actomyosin V. (A) [MantADP] dependence of the fast observed rate constants for mantADP binding to myosin V in 2 mM EDTA (●), actomyosin V in 2 mM EDTA (□), myosin V in the presence of 2 mM free Mg^{2+} (▲), and actomyosin V in 2 mM Mg^{2+} (○). The solid lines are the best linear fits of the data. (B) [MantADP] dependence of the slow observed rate constants for mantADP binding to myosin V (◆) and actomyosin V (□) in the presence of 2 mM free Mg^{2+}. The solid lines are the best linear fits of the data.

are ~0.4−3 s^{-1} and show a weak dependence on the [mantADP] (Figure 5B).

In the absence of magnesium, the second-order association rate constant for mantADP binding to myosin V is 9.2 ± 0.2 μM^{-1} s^{-1} (Figure 5A, Table 1). The dissociation rate constant of cation-free mantADP estimated from the *y*-intercept (k_{-mD}) is 46.3 ± 2.3 s^{-1} (Figure 5A), comparable to the value measured directly by competition of mantADP

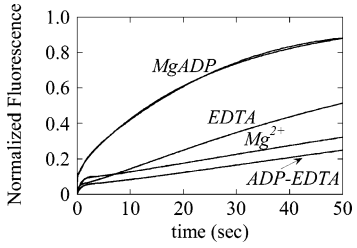

FIGURE 6: Kinetics of myosin V and myosin V−ADP dissociation from actin filaments (±Mg^{2+}). Time courses of fluorescence change upon mixing 12 μM unlabeled actin with an equal volume of (curve *MgADP*) 0.6 μM pyrene actomyosin V and 2 mM ADP (final conditions: K50 buffer, 5 mM free Mg^{2+}), (curve *Mg^{2+}*) 0.6 μM pyrene actomyosin V (final conditions: K50 buffer, 5 mM free Mg^{2+}), (curve *ADP-EDTA*) 0.6 μM pyrene actomyosin V and 2 mM ADP (final conditions: K50 buffer, 4 mM EDTA), or (curve *EDTA*) 0.6 μM pyrene actomyosin V (final conditions: K50 buffer, 4 mM EDTA). The smooth lines through the data represent best fits to double exponentials. The data traces represent the averages of 3−6 individual transients.

with unlabeled ADP (47.3 ± 1.3 s^{-1}, Figure 2A) and from the best fit of the [Mg^{2+}] dependence of the mantADP dissociation rates to eq 5 (42.0 ± 1.4 s^{-1}, Figure 3A).

D. MantADP Binding to Actomyosin V. Time courses of MgmantADP binding to actomyosin V are biphasic. The second-order association rate constant ($k'_{+Mg.mD}$) obtained from the slope of the fast phase (Figure 5A) is 6.2 ± 0.6 μM^{-1} s^{-1} (Table 2), within a factor of 2 of published values under comparable conditions (*7*, *9*, 13). The dissociation rate constant of Mg^{2+}mantADP ($k'_{-Mg.mD}$) estimated from the *y*-intercept is indistinguishable from the origin. In the presence of saturating magnesium, the observed rate constants of the slow phases are ~0.5 s^{-1} and do not display a strong [mantADP] dependence (Figure 5B).

In the absence of magnesium, the slow phase is less than 10% of the overall signal, consistent with a small population of the strong MgADP binding state. The second-order association rate constant is k'_{+mD} = 10.2 ± 0.7 μM^{-1} s^{-1} (Figure 5A, Table 2). The dissociation rate constant of cation-free mantADP (k'_{-mD}) estimated from the *y*-intercept is 39.7 ± 5.1 s^{-1} (Figure 5A), comparable to the value measured directly by competition unlabeled ADP with mantADP in the presence of excess EDTA and no added Mg^{2+} (44.7 ± 1.0 s^{-1}, Figure 2B), and from the *y*-intercept value ([Mg^{2+}] = 0) of the best fit to the [Mg^{2+}] dependence of the mantADP dissociation rates to eq 5 (46.2 ± 1.5 s^{-1}, Figure 3A).

E. Determination of Mg^{2+} Affinity for ADP. By isothermal titration calorimetry the affinity of ADP for Mg^{2+} under our experimental conditions (K50 buffer, pH 7.0, 25 °C) is 350 ± 30 μM (Tables 1 and 2).

F. Myosin V Dissociation from Pyrene Actin Filaments. Strongly bound myosin V quenches the fluorescence of pyrene actin ~70% (*7*). Dissociation of strongly bound myosin V from pyrene actin filaments was measured by competition with unlabeled actin. Time courses of fluorescence change under all conditions examined (2 mM ADP + 5 mM Mg^{2+}, 2 mM ADP + 4 mM EDTA, 5 mM Mg^{2+}, and 4 mM EDTA) are biphasic with 5−11% of fast phase (Figure 6). The majority of actomyosin dissociation is slow with observed rate constants ranging from 0.006 to 0.039 s^{-1}. MgADP increases the dissociation rate constant of actomyosin (Table 3). The dissociation rate constants and amplitudes

Table 3: Summary of the Rate Constants and Amplitudes of Actomyosin V Dissociation

	2 mM ADP, 5 mM Mg^{2+}	2 mM ADP, 4 mM EDTA	4 mM EDTA	5 mM Mg^{2+}
A_{ds}[a] (%)	90	95	89	91
k_{df}[a] (s^{-1})	21.4 ± 0.62	1.8 ± 0.03	1.2 ± 0.02	1.7 ± 0.03
k_{ds}[a] (s^{-1})	0.039 ± 0.0002	0.006 ± 0.0001	0.023 ± 0.001	0.007 ± 0.0001
k_-^w[b] (s^{-1})	21.0	1.69	1.02	1.63
k_-^s[b] (s^{-1})	0.040	0.006	0.027	0.007
k_+^s[b] (s^{-1})	0.35	0.11	0.18	0.07
$K_A^s = k_-^s/k_+^s$	0.113	0.056	0.149	0.104

[a] k_{df}, k_{ds}, and A_{ds} are the observed fast rate constant, slow rate constant, and slow phase amplitude. [b] k_-^w, k_-^s, and k_+^s are fundamental rate constants defined by Scheme 4.

Scheme 3

$$\begin{array}{ccc} AM^w.(L) & \underset{k_+^w}{\overset{k_-^w}{\rightleftharpoons}} & A + M^w.(L) \\ \uparrow\downarrow & & \\ AM^s.(L) & \underset{k_+^s}{\overset{k_-^s}{\rightleftharpoons}} & A + M^s.(L) \end{array}$$

Scheme 4

$$AM^s.(L) \underset{k_+^s}{\overset{k_-^s}{\rightleftharpoons}} AM^w.(L) \underset{k_+^w}{\overset{k_-^w}{\rightleftharpoons}} A + M^w.(L)$$

of the fast (k_{df}, A_{df}) and slow phases (k_{ds}, A_{ds}), for each condition examined are listed in Table 3.

The biphasic dissociation time course suggests that there are two conformations of actomyosin V with quenched pyrene fluorescence: a strong actin-binding conformation (AM^s), and a weak actin-binding conformation (AM^w), which allows two distinct mechanisms for actomyosin V dissociation. Dissociation can follow either a parallel dissociation mechanism (Scheme 3) or a sequential mechanism via isomerization from the strong (AM^s) to weak (AM^w) actin-binding conformation before dissociation (Scheme 4). In Schemes 3 and 4, (L) represents optional bound ligands (ADP and/or Mg^{2+}). The unquenched collision complexes (*15*, *16*) are omitted for simplicity. Note that these are two quenched pyrene actomyosin states that are considered "strongly bound" using the terminology of Geeves (*15*, *17*).

Determination of the scheme that accurately describes actomyosin V dissociation requires the following considerations. The observed 90−95% slow phase implies that the majority of actomyosin V is in the strong actin-binding conformation (AM^S) at equilibrium ($t = 0$) and that interconversion between the two conformations is negligible. The parallel scheme (Scheme 3) predicts that the two actomyosin conformations dissociate independently. Because dissociation of actomyosin V−ADP is biphasic, if the parallel scheme applied, time courses of myosin V−ADP binding to actin filaments would also be biphasic with amplitudes equivalent to those measured from dissociation (i.e. 5−11% fast and 89−95% slow phase, see Table 3), but this is not observed (discussed below, binding displays either no slow phase or 68−77% fast phase). Therefore, we favor the sequential reaction mechanism to describe the reaction mechanism of actomyosin V dissociation.

Fast dissociation is about 2 orders of magnitude more rapid than slow dissociation ($k_-^w \gg k_-^s$; Table 3). Solving Scheme 4 under the condition $k_-^w \gg k_-^s$ and $k_+^w = 0$ (irreversible release, fulfilled by mixing with excess unlabeled actin), with the initial population distributed between AM^s and AM^w species only, the fast (k_{df}) and slow (k_{ds}) observed dissociation rate constants and the fast phase amplitude (A_{df}) can be expressed in terms of the fundamental rate constants defined in Scheme 4 as follows (see Appendix):

$$k_{df} = k_-^w + k_+^s$$

$$k_{ds} = \frac{k_-^s k_-^w}{k_-^w + k_+^s}$$

$$A_{df} = \left(\frac{k_-^s}{k_-^s + k_+^s}\right)\left(\frac{k_-^w}{k_-^w + k_+^s}\right) \quad (7)$$

The fundamental rate constants calculated by eq 7 are summarized in Table 3.

G. Myosin V Binding to Actin Filaments. Time courses of myosin−ADP and myosin−MgADP binding to pyrene actin filaments follow double exponentials with slow phases that comprise 23−32% of the total amplitude (Figure 7A). Time courses of myosin binding in the absence of ADP (with and without Mg^{2+}, Figure 7A) follow double exponentials with a small slow phase comprising less than 5% of the total amplitude. The observed rate constants of the fast phases (k_{bf}) depend linearly on the actin concentration (Figure 7B,C). Solving Scheme 4 where $k_+^w[A] \gg k_+^s$ with initial population of A + M·(L) states only yields (see Appendix)

$$k_{bf} = k_+^w[A] + k_-^w$$

$$k_{bs} = k_-^s + \frac{k_+^s k_+^w[A]}{k_+^w[A] + k_-^w} \quad (8)$$

where k_{bf} and k_{bs} are fast and slow binding observed rate constants, respectively. Thus, the rate constants defined in Scheme 4 for binding (k_+^w) and dissociation ($k_-^{w\dagger}$, superscript † is used to distinguish from k_-^w for pyrene actin dissociation measured directly by competition with unlabeled actin, Table 3) from the weak actin-binding state ($AM^w.(L)$) can be obtained from the slope and *y*-intercept of the linear fit from the [actin] dependence of the observed fast phase, respectively (Figure 7C). The observed rate constants of the slow phases (k_{bs}) should be hyperbolic ($k_{bs} \sim 1-2\ s^{-1}$) but display little actin concentration dependence indicating that binding to the weak states is more rapid than dissociation from the weak binding states ($k_+^w[A] \gg k_-^w$). The rate and equilibrium constants under all conditions examined (2 mM ADP + 3 mM Mg^{2+}, 2 mM ADP + 2 mM EDTA, 3 mM

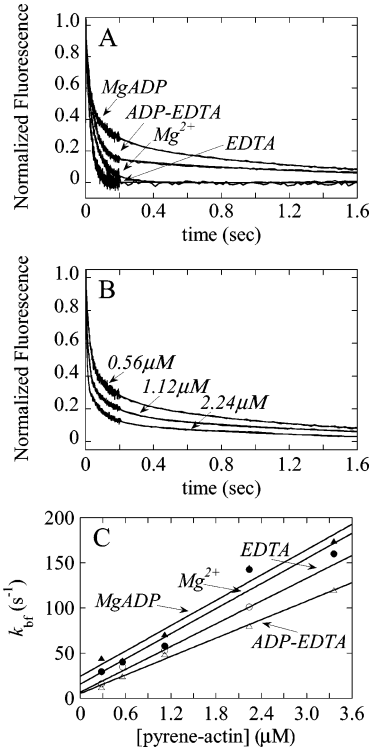

FIGURE 7: Kinetics of myosin V and myosin V−ADP binding to actin filaments (±Mg^{2+}). (A) Time courses of fluorescence change upon mixing 0.56 μM pyrene actin filaments with (curve *MgADP*) 0.056 μM myosin V and 4 mM ADP (final conditions: K50 buffer, 3 mM free Mg^{2+}), (curve *Mg^{2+}*) 0.056 μM myosin V (final conditions: K50 buffer, 3 mM free Mg^{2+}), (curve *ADP-EDTA*) 0.056 μM myosin V and 4 mM ADP (final conditions: K50 buffer, 4 mM EDTA), and (curve *EDTA*) 0.056 μM myosin V (final conditions: K50 buffer, 4 mM EDTA). The smooth lines through the raw data are the best fits to double exponentials (curves *MgADP*, *ADP-EDTA*) and double exponentials with small slow phases (curves *Mg^{2+}*, *EDTA*). (B) Time courses of fluorescence change upon mixing various concentrations of 10-fold excess pyrene actin filaments (0.56 μM, 1.12 μM, and 2.24 μM) with myosin V (0.056 μM, 0.11 μM, and 0.22 μM, respectively) and 4 mM ADP (final conditions: K50 buffer, 3 mM free Mg^{2+}). (C) Dependence of the observed fast binding rate constant (k_{bf}) for myosin V on pyrene actin filament concentration.

Table 4: Summary of the Rate Constants and Amplitudes of Actomyosin V Binding

	2 mM ADP, 3 mM Mg^{2+}	2 mM ADP, 2 mM EDTA	2 mM EDTA	3 mM Mg^{2+}
A_{bs}[a] (%)	32	23	nd[c]	nd
k_+^w [b] (μM^{-1} s^{-1})	48.8 ± 4.8	34.1 ± 1.4	42.1 ± 2.5	46.4 ± 6.2
$k_-^{w\dagger}$ [b] (s^{-1})	24.4 ± 9.2	5.4 ± 2.6	6.9	15.9 ± 11.8
k_{bs}[a] (s^{-1})	~10	~1	nd	nd
$K_A^w = k_-^w/k_+^w$ (μM)	0.431	0.049	0.024	0.035
$K_{A,overall}$ (μM)	0.044	0.0026	0.0031	0.0033

[a] k_{bs} and A_{bs} is the observed rate constant of slow phase and fast phase amplitude. [b] k_+^w and $k_-^{w\dagger}$ are fundamental rate constants defined by Scheme 4. The superscript † is used here to distinguish k_-^w measured from pyrene actin release (Table 3). The k_-^w used to calculate K_A^w is from pyrene actin release (from Table 3). [c] Not determined

Mg^{2+}, and 2 mM EDTA) are summarized in Table 4. We used the values (k_-^w) measured directly from dissociation experiments for calculating the equilibrium constants (Table 4) because the weak binding state dissociation rate constants ($k_-^{w\dagger}$) obtained from the *y*-intercept are subject to large uncertainties (Table 4).

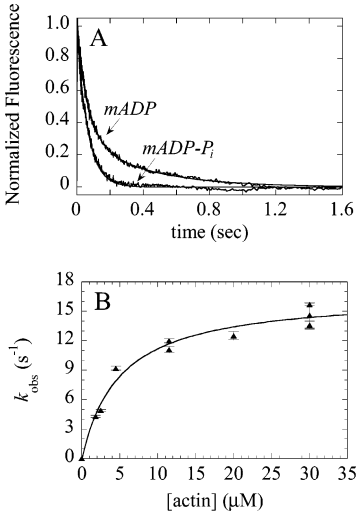

FIGURE 8: Kinetics of product release from actomyosin V−ADP and actomyosin V−ADP−P_i. (A) Time courses of fluorescence change upon first mixing myosin V with mantADP (*mADP*) or mantATP (*mADP-P_i*), aging ~2 s, then mixing with actin filaments and excess MgADP in K50 containing ≥2 mM $MgCl_2$ (saturating) with the stopped flow in sequential mix mode. Final concentrations are 0.67 μM myosin V, 33 μM fluorescent nucleotide, 30 μM actin filaments, and 2 mM MgADP. The smooth lines through the data represent best fits to single (curve *mADP-P_i*) or double (curve *mADP*) exponentials. The data traces represent unaveraged data (curve *mADP-P_i*) or the average of two individual transients (curve *mADP*). (B) Dependence of the observed rate constant (k_{obs}) for product release of mantADP.P_i from actomyosin V as a function of actin filament concentration.

H. Actin-Activated Product Release from Myosin V. The maximum actin-activated steady-state ATPase rate of myosin V (k_{cat}) in the presence of ≥1 mM free Mg^{2+} is 12−16 s^{-1} $head^{-1}$ (*7*, *9*) (data not shown), suggesting that the slow (~1 s^{-1}) actomyosin−ADP isomerization is not along the predominant ATPase cycle reaction pathway. One possibility is that the slow isomerization reflects an off-pathway kinetic transition. To test this possibility we measured the rate of actin-activated mantADP and mantADP−P_i dissociation from myosin V (Figure 8).

Time courses of actin-activated mantADP release are biphasic, consistent with the formation of two myosin−ADP states. The observed rate constants of the fast and slow phases are comparable to those measured by competing bound mantADP from actomyosin (Figures 2 and 3). In contrast, time courses of mantADP−P_i dissociation follow single exponentials (Figure 8A) with observed rate constants that depend hyperbolically on the actin filament concentration (Figure 8B). The maximum rate constant of mantADP release from actomyosin V−mantADP−P_i is ~16 s^{-1}, comparable to the maximum steady-state ATPase turnover rate and dissociation of MgmantADP from the weak ADP binding states, suggesting that, under these experimental conditions, where there is no load on the actomyosin complex, the slow isomerization observed with mantADP does not occur along the ATPase cycle reaction pathway. This suggests that, in the absence of load, the strong ADP binding state (AM.Mg.mD$^{\alpha}$) is not significantly populated during the steady-state actomyosin V ATPase cycle.

DISCUSSION

A. Evidence for Multiple Myosin V−ADP and Actomyosin V−ADP States. The biphasic MgADP binding and dissociation time courses are consistent with two stable ADP bound myosin V and actomyosin V states that are in reversible equilibrium. One state (M.Mg.mD$^{\beta}$) readily exchanges nucleotide and cation. The second (M.Mg.mD$^{\alpha}$) binds nucleotide and cation strongly. The M.Mg.mD$^{\alpha}$−M.Mg.mD$^{\beta}$ isomerization equilibrium constant is near unity ($K_{isom,Mg}$ = 0.59, $K'_{isom,Mg}$ = 3.8, Tables 1 and 2), indicating that the two states are of comparable energies and populated under equilibrium conditions. However, the slow rate constants for isomerization indicate a reasonably large activation energy barrier.

Actin binding weakens the Mg^{2+} affinity 2-fold and shifts the isomerization equilibrium ($K'_{isom,Mg}$ = 3.8, Table 2) to favor population of the weak ADP binding state (AM.Mg.mD$^{\beta}$ in Scheme 2), favoring dissociation of divalent-cation-free ADP and weakening the overall binding affinity of MgADP. Actin does not weaken the affinity or accelerate the release of cation-free ADP, indicating that the coupling of actin and ADP binding sites requires bound Mg^{2+}.

Recently a manuscript characterizing the effect of magnesium on myosin V ADP binding was published (*18*). The majority of our measurements are in general agreement. However, that study concluded that both myosin−MgADP and actomyosin−MgADP states readily exchanged bound magnesium. We did not observe a [Mg^{2+}] dependence of the slow phase for ADP binding to myosin V or actomyosin V and favor a mechanism where the strong ADP binding states of myosin V and actomyosin V do not exchange bound Mg^{2+}.

B. Overall MgmantADP Binding to Myosin V and Actomyosin V at Saturating [Mg^{2+}]. The overall dissociation equilibrium constant for myosin V−MgADP ($K_{Mg.mD,overall}$) is defined as

$$K_{Mg.mD,overall} = \frac{[M][Mg.mD]}{([M.Mg.mD^{\alpha}] + [M.Mg.mD^{\beta}])} \quad (9)$$

The equilibrium concentrations of strong (α) and weak (β) ADP binding states are determined by [myosin], [nucleotide], and the equilibrium constants for ADP binding ($K_{Mg.mD}$) and isomerization ($K_{isom,Mg}$) from the strong ADP binding state to the weak ADP binding state according to

$$[M.Mg.mD^{\beta}] = \frac{1}{K_{Mg.mD}}[M][Mg.mD] \quad (10)$$

and

$$[M.Mg.mD^{\alpha}] = \frac{1}{K_{isom,Mg}}[M.Mg.mD^{\beta}] \quad (11)$$

The sum of the two myosin−MgADP states is

$$[M.Mg.mD^{\alpha}] + [M.Mg.mD^{\beta}] = \frac{1}{K_{Mg.mD}}\left(1 + \frac{1}{K_{isom,Mg}}\right)[M][Mg.mD] \quad (12)$$

Therefore, $K_{Mg.mD,overall}$ can be expressed in terms of the individual equilibrium binding constants as follows:

$$K_{Mg.mD,overall} = K_{Mg.mD}\left(\frac{K_{isom,Mg}}{1 + K_{isom,Mg}}\right) \quad (13)$$

The coefficient $K_{isom,Mg}/(1 + K_{isom,Mg})$ accounts for contributions of the isomerization equilibrium to the overall ADP affinity.

Similarly, the overall ADP dissociation equilibrium constant from actomyosin V in the presence of saturating Mg^{2+} ($K'_{Mg.mD,overall}$) can be calculated from

$$K'_{Mg.mD,overall} = K'_{Mg.mD}\left(\frac{K'_{isom,Mg}}{1 + K'_{isom,Mg}}\right) \quad (14)$$

The overall affinity of ADP binding to myosin V ($K_{Mg.mD,overall}$) is 0.7 μM, and that of actomyosin V ($K'_{Mg.mD,overall}$) is 1.8 μM (Tables 1 and 2). Therefore, actin weakens overall MgADP binding to myosin V by a factor of 2.7 ($K'_{Mg.mD,overall}/K_{Mg.mD,overall}$ = 2.7).

C. Mechanism of Actin Binding to Myosin V. Actomyosin V dissociation kinetics indicate that myosin release is biphasic, consistent with two *quenched* pyrene actomyosin V states ("strongly" bound and "weakly" bound). At equilibrium, the majority of actomyosin V is in the strong actin-binding conformation as indicated by the >90% slow phase amplitude. Consequently, we favor a sequential mechanism for strongly bound myosin V dissociation from actin where actomyosin V isomerizes from the strong to the weak actin-binding conformation before dissociation. We should point out that these are two quenched pyrene actomyosin states and are therefore different from the A and R states of Geeves et al. (*15*, *16*) where the A state is an unquenched pyrene actomyosin state.

Similar to overall ADP binding to myosin V and actomyosin V, the overall dissociation equilibrium constant for myosin V from actin is

$$K_{A,overall} = K_A^w\left(\frac{K_A^s}{1 + K_A^s}\right) \quad (15)$$

where K_A^s is the equilibrium constant for interconversion from the strong to the weak actin-binding state (Table 3) and K_A^w is the dissociation equilibrium constant for weak actin binding (Table 4). MgADP weakens the affinity of myosin V for actin ~14-fold (Table 4). ADP or Mg^{2+} alone has minimal (<2-fold) effects on actin binding (Table 4), which suggests that cation and nucleotide together (MgADP) weaken acting binding to myosin V dramatically.

It is possible that the two quenched actin-binding states (AM^{w}.(Mg).ADP and AM^{s}.(Mg).ADP) represent the two mantADP isomerization states (AM.(Mg).mD$^{\alpha}$ and AM.(Mg).mD$^{\beta}$, respectively). However, the interconversion rate constants from the two quenched actin-binding states (k_+^s and k_-^s in Scheme 4) are different from the mantADP isomerization rate constants (k'_{-isom} (k_{-isom}) and k'_{+isom} (k_{+isom}) in Schemes 1 and 2), suggesting that the quenched actomyosin V conformations are distinct from the myosin V−mantADP isomerization states.

A pertinent question is to define which ADP-binding isomerization state the M.(Mg).ADP complex populates when binding and dissociating from actin. Our results indicate that, at equilibrium and in the presence of Mg^{2+}, the majority of actomyosin V is in the weak ADP binding

Scheme 5

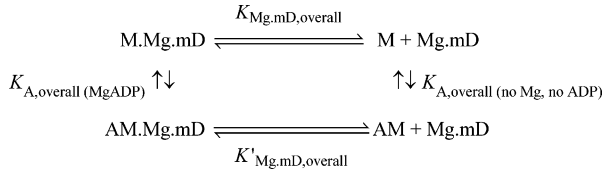

Scheme 6

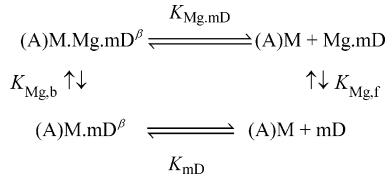

state (AM.Mg.mD$^{\beta}$), and the majority of myosin V is in the strong ADP binding state (M.Mg.mD$^{\alpha}$). We therefore conclude that the strong ADP binding state of myosin V (M.Mg.mD$^{\alpha}$) binds actin and that dissociation occurs mostly from the weak ADP binding state (AM.Mg.mD$^{\beta}$). Furthermore, in the absence of Mg^{2+}, the strong ADP binding states of both actomyosin V and myosin V are not significantly populated, requiring that myosin V bind and dissociate only from the weak ADP binding states (M.mD$^{\beta}$ or AM.mD$^{\beta}$).

D. Thermodynamic Balance of the Actomyosin V Interaction with ADP. Previous studies on the interaction of ADP and actomyosin V used four equilibrium constants to define the interaction of myosin V, MgADP, and actin (*7*). This model implicated a single myosin V−ADP and a single actomyosin V−ADP state, and the product of the equilibrium constants deviated greatly from the predicted value of 1. It was suggested that unresolved actomyosin ADP binding states could account for the discrepancy in the thermodynamic linkage (*7*).

In the present work, we identify two isomerization states for myosin V−ADP and two actomyosin V−ADP conformations and can now define the *overall* interaction of myosin V-1IQ with MgADP and actin filaments as shown in Scheme 5. In Scheme 5, M.Mg.mD and AM.Mg.mD represent both ADP states and AM represents both actomyosin V conformations. Using our overall equilibrium constants (Scheme 5), which incorporate the contribution of the ADP isomerization and the two actomyosin V conformations, we obtain a product (clockwise in Scheme 5) of 5.3. This value approaches unity more closely than previous analysis. However, the discrepancy in the thermodynamic linkage could be significant, and additional states, such as the actin-binding states described by Geeves (*15*) or the ADP states identified by Rosenfeld with smooth muscle myosin II (*19*), may exist and may contribute to the energetic imbalance if they are populated and cannot be fully resolved with our current measurements.

In the absence of magnesium, the ADP isomerization states M.mD$^{\alpha}$ and AM.mD$^{\alpha}$ are not significantly (≤10%) populated so the overall ADP dissociation equilibrium constants (Scheme 5) reduce to K_{mD} and K'_{mD}. The product of the equilibrium constants in Scheme 5 in the absence of Mg^{2+} is 1.2.

Similarly, the interaction of ADP, myosin V, and Mg^{2+}, in the presence and absence of actin, is defined as shown in Scheme 6. The products of the equilibrium constants (from Tables 1 and 2) in Scheme 6 are 1.6 and 2.1, in the presence of saturating magnesium and in the absence of magnesium, respectively.

Scheme 7

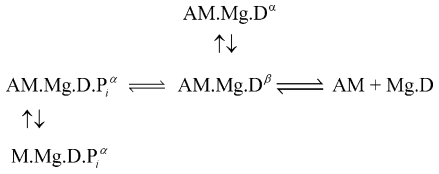

In summary, the rate and equilibrium constants obtained in this study provide a sound description, within reasonable error, of the myosin, ADP, and actin binding linkage consistent with the principles of thermodynamics.

E. Pathway of Product Dissociation in the Actomyosin V Steady-State ATPase Cycle. Actin-activated mantADP release from myosin−MgmantADP−P_i, but not myosin−MgmantADP, does not show a slow phase, suggesting that, under the conditions of no load, the myosin−MgmantADP isomerization and the M.Mg.mD$^{\alpha}$ intermediate are off the main ATPase cycle reaction pathway. However, under high load, the velocity of actomyosin V is reduced (*20*) and the dwell times between processive steps are increased (*21*). We predict that, in response to an external load, population of the strongly bound actomyosin V ADP state (AM.Mg.D$^{\alpha}$) prolongs the lifetime of the force-generating step, as has been suggested for several other myosins (*22, 23*).

In addition, there may be another role for the strongly bound ADP state of actomyosin V (AM.Mg.D$^{\alpha}$). Under conditions where ADP can rebind actomyosin V, the slow isomerization may be relevant. Under physiological nucleotide concentrations (mM ATP, μM ADP) the probability of ADP binding to single-headed myosin V is small (*12*). However, modeling of myosin V processive run lengths (*24*) suggests that ATP binding to the trailing head is slow (<0.1 μM^{-1} s^{-1}), raising the possibility that ADP rebinds and contributes to termination of a processive run. Therefore, under high concentrations of ADP, the strongly bound ADP state (AM.Mg.D$^{\alpha}$) may become significantly populated and result in a stalling or termination of the processive run.

We favor a pathway (Scheme 7) for the myosin V ATPase cycle where binding of myosin-MgADP−P_i to actin induces closure the actin-binding cleft and movement of Switch I (*25, 26*) which disrupts magnesium coordination and accelerates P_i release, generating the weak ADP binding state that readily exchanges bound magnesium (AM.Mg.mD$^{\beta}$), as shown in Scheme 7, where α is used to represent a state that exchanges magnesium slowly and β is used to represent a state that readily exchanges magnesium (collision complexes are omitted from the reaction scheme for clarity).

This mechanism is significantly different from a published model of ADP release (*18*), where actomyosin V−ADP enters a strong ADP binding state following P_i release and the ADP release pathway follows AM.Mg.mD$^{\alpha}$ → AM.mD$^{\alpha}$ → AM.mD$^{\beta}$ → AM + mD in the presence of saturating magnesium (i.e. magnesium is released first, and then ADP dissociates as a cation-free species). The rate-limiting step in this pathway is AM.mD$^{\alpha}$ → AM.mD$^{\beta}$, reported as k_{-isom} = 40 s^{-1} (Figure 7 in ref *18*), which implies that the ~16 s^{-1} turnover rate of actomyosin V is not limited by ADP release from actomyosin.

F. Comparison to Other Myosins. The existence of multiple actomyosin−ADP states has been identified in other

myosins including brush border actomyosin I (*27*), smooth muscle myosin II (*19*), and myosin X (*28*), but the magnesium dependence of the stabilities of these states has not been investigated.

In addition, several studies have identified two ADP-bound states of fast skeletal muscle myosin (II) subfragment-1 (S1) (*29*−*37*), and of the ternary actoS1.ADP complex (*38*−*40*). A four-step mechanism for the interaction of S1 with actin has been proposed by Conibear (*23*), where formation of a diffusion-limited collision complex is followed by two consecutive isomerizations with increasing actin affinity. The first isomerization is thought to reflect a stereospecific binding event (collision complex transition to A state), and the second isomerization (transition between two R states) to represent the force-generating conformational changes involving the shifting of the S1 regulatory domain, or lever arm (*41*), which has been observed directly in structural studies (*42, 43*). The mechanism of Conibear builds upon models proposed by Taylor (*44*), White (*45*), and Geeves (*39*) and suggests that the two actoS1.ADP states of the second isomerization may have a role in prolonging the actomyosin crossbridge in the presence of a load (*23*). If the second isomerization states for fast skeletal muscle are akin to the two actomyosin V−ADP states we report here (AM.Mg.D$^{\alpha}$ and AM.Mg.D$^{\beta}$), then it is plausible that the actomyosin V strong ADP-binding state (AM.Mg.D$^{\alpha}$) serves to maintain strong binding of ADP by actomyosin V under load.

In the absence of actin, fast skeletal muscle myosin II (S1) does not exchange bound Mg^{2+} with solution (*46, 47*). Therefore, in the absence of actin, skeletal muscle myosin II predominantly populates a strong-binding MgADP state (α state). However, actin weakens the ADP binding affinity of skeletal muscle myosin II more than 100-fold (*48*). An actin-induced disruption of Mg^{2+} coordination, binding affinity, and shift in the equilibrium among myosin−MgADP states to favor a weakly bound ADP state (β state) may account for the weak ADP binding affinity and accelerated dissociation rate constant of ADP from actomyosin II, similar to actomyosin V.

G. Structural Implications. The crystal structure of myosin V suggests that closure of the actin-binding cleft is coupled to the opening of Switch 1 (*25*). Since Ser218 of Switch 1 helps coordinate bound magnesium, actin binding and subsequent actin-binding cleft closure would disrupt Mg^{2+} coordination, weaken Mg^{2+} binding, and shift the isomerization to favor weak ADP binding, and thus accelerate overall ADP release from myosin V.

Recently, a structure of myosin V was obtained by soaking crystals of nucleotide-free myosin V with MgADP (*26*). In this structure, Lys169 of the P-loop is not in position to coordinate the β-phosphate of ADP, and the Mg^{2+} binding site is vacant because Ser218 of Switch 1 is not oriented properly to coordinate the bound cation. It is likely that this structure represents an intermediate, presumably a collision complex (*12*) that is capable of accommodating nucleotide, preceding formation of the weak ADP binding state of myosin V (M.mD$^{\beta}$ in Scheme 1). Formation of M.mD$^{\beta}$ (and AM.mD$^{\beta}$) is likely to involve reorganization of the P-loop so that it can interact with the β-phosphate of ADP, accounting for the reasonably slow ADP dissociation rate constant, even in the absence of bound cation (Tables 1 and 2). The reorganization of the P-loop with formation of the β states would generate a small rotation of the lever arm. A subsequent conformational change ("closing") of Switch 1 would help coordinate the bound magnesium and favor formation of the α states, presumably opening the actin-binding cleft and weakening the affinity for actin.

ACKNOWLEDGMENT

We are grateful to Dr. Arnon Henn for many insightful discussions and his generous assistance with cell culture and baculovirus expression. We also thank anonymous reviewers for critical evaluation of the manuscript.

APPENDIX

A1. Two-Step Sequential Binding Mechanism. The 2-step sequential mechanism (ignoring collision complex formation) for ligand (L) binding to myosin (M) is defined by Scheme A1, where L represents ADP or actin, M·L is the strong L

Scheme A1

$$\mathrm{M\cdot L} \underset{k_{+\mathrm{isom}}}{\overset{k_{-\mathrm{isom}}}{\rightleftharpoons}} \mathrm{M\cdot(L)} \underset{k+}{\overset{k_-}{\rightleftharpoons}} \mathrm{M + L}$$

binding state, M·(L) is the weak L binding state, and M + L represent dissociated states. The differential equations corresponding to Scheme A1 are

$$\frac{\mathrm{d[M\cdot L]}}{\mathrm{d}t} = -k_{-\mathrm{isom}}[\mathrm{M\cdot L}] + k_{+\mathrm{isom}}[\mathrm{M\cdot(L)}] \quad \text{(A1)}$$

$$\frac{\mathrm{d[M\cdot(L)]}}{\mathrm{d}t} = k_{-\mathrm{isom}}[\mathrm{M\cdot L}] - k_{+\mathrm{isom}}[\mathrm{M\cdot(L)}] - k_-[\mathrm{M\cdot(L)}] + k_+[\mathrm{M}][\mathrm{L}] \quad \text{(A2)}$$

$$\frac{\mathrm{d[M]}}{\mathrm{d}t} = k_-[\mathrm{M\cdot(L)}] - k_+[\mathrm{M}][\mathrm{L}] \quad \text{(A3)}$$

Two of the above differential equations are independent. The third equation is dependent because it can be derived from the two independent equations by making use of mass conservation ([M·L] + [M·(L)] + [M] = 1). Under pseudo-first-order conditions ([L] ≫ [M]) the concentration of ligand [L] can be considered constant. Applying mass conservation ([M] = 1 − [M·L] − [M·(L)]), eq A2 can be expressed as

$$\frac{\mathrm{d[M\cdot(L)]}}{\mathrm{d}t} = k_{-\mathrm{isom}}[\mathrm{M\cdot L}] - k_{+\mathrm{isom}}[\mathrm{M\cdot(L)}] - k_-[\mathrm{M\cdot(L)}] + k_+[\mathrm{L}](1 - [\mathrm{M\cdot L}] - [\mathrm{M\cdot(L)}]) \quad \text{(A4)}$$

and rearranged to

$$\frac{\mathrm{d[M\cdot(L)]}}{\mathrm{d}t} = (k_{-\mathrm{isom}} - k_+[\mathrm{L}])[\mathrm{M\cdot L}] - (k_{+\mathrm{isom}} + k_- + k_+[\mathrm{L}])[\mathrm{M\cdot(L)}] + k_+[\mathrm{L}] \quad \text{(A5)}$$

Equations A1 and A5 can be rearranged and expressed as

$$\begin{cases} \left(\frac{\mathrm{d}}{\mathrm{d}t} + k_{-\mathrm{isom}}\right)[\mathrm{M\cdot L}] - k_{+\mathrm{isom}}[\mathrm{M\cdot(L)}] = 0 \\ -(k_{-\mathrm{isom}} - k_+[\mathrm{L}])[\mathrm{M\cdot L}] + \\ \quad \left(\frac{\mathrm{d}}{\mathrm{d}t} + k_{+\mathrm{isom}} + k_- + k_+[\mathrm{L}]\right)[\mathrm{M\cdot(L)}] = k_+[\mathrm{L}] \end{cases} \quad \text{(A6)}$$

The second-order polynomial equation ($ax^2 + bx^1 + c = 0$) for the eigenvalues (rate constants) of the expressions in eq

A6 can be obtained by setting the determinant equal to zero:

$$\begin{vmatrix}(-\lambda + k_{-\text{isom}}) & (-k_{+\text{isom}}) \\ (-k_{-\text{isom}} + k_{+}[\text{L}]) & (-\lambda + k_{+\text{isom}} + k_{-} + k_{+}[\text{L}])\end{vmatrix} = 0 \quad \text{(A7)}$$

which can be expanded into

$$(\lambda - k_{-\text{isom}})(\lambda - k_{+\text{isom}} - k_{-} - k_{+}[\text{L}]) - (-k_{+\text{isom}})(-k_{-\text{isom}} + k_{+}[\text{L}]) = \lambda^2 - (k_{+\text{isom}} + k_{-\text{isom}} + k_{-} + k_{+}[\text{L}])\lambda + k_{-\text{isom}}k_{-} + k_{-\text{isom}}k_{+}[\text{L}] + k_{+\text{isom}}k_{+}[\text{L}] = 0 \quad \text{(A8)}$$

Two rate constants (eigenvalues λ_1 and λ_2) are obtained by solving eq A8:

$$\lambda = \lambda_{1,2} = \frac{b \pm \sqrt{b^2 - 4c}}{2} \quad \text{(A9)}$$

with

$$\begin{cases} b = k_{+\text{isom}} + k_{-\text{isom}} + k_{-} + k_{+}[\text{L}] \\ c = k_{-\text{isom}}k_{-} + k_{-\text{isom}}k_{+}[\text{L}] + k_{+\text{isom}}k_{+}[\text{L}] \end{cases} \quad \text{(A10)}$$

The general solution for eq A6 is determined by the two eigenfunctions (one column matrix in the first two terms) and a special solution (third term) of eq A6:

$$\begin{pmatrix}[\text{M}\cdot\text{L}] \\ [\text{M}\cdot(\text{L})]\end{pmatrix} = C_1\begin{pmatrix}1 \\ \dfrac{-\lambda_1 + k_{-\text{isom}}}{k_{+\text{isom}}}\end{pmatrix}e^{-\lambda_1 t} + C_2\begin{pmatrix}1 \\ \dfrac{-\lambda_2 + k_{-\text{isom}}}{k_{+\text{isom}}}\end{pmatrix}e^{-\lambda_1 t} + \frac{k_{+}[\text{L}]}{c}\begin{pmatrix}k_{+\text{isom}} \\ k_{-\text{isom}}\end{pmatrix} \quad \text{(A11)}$$

The c term in eq A11 is defined by eq A10. C_1 and C_2 are arbitrary constants that are determined by the initial partitioning of [M·L] and [M·(L)] at $t = 0$.

Case 1: Ligand (L) Dissociation from Myosin. In measurements of ligand (L) dissociation kinetics, excess unlabeled ligand competes with labeled ligand and makes dissociation irreversible ($k_{+} = 0$). In this case, the two rate constants (λ_1 and λ_2) from eq A9 are

$$\lambda = \lambda_{1,2} = \frac{1}{2}(k_{+\text{isom}} + k_{-\text{isom}} + k_{-} \pm \sqrt{(k_{+\text{isom}} + k_{-\text{isom}} + k_{-})^2 - 4k_{-\text{isom}}k_{-}}) \quad \text{(A12)}$$

Under conditions where $k_{-} \gg k_{-\text{isom}}$, λ_1 and λ_2 simplify to

$$\begin{cases} \lambda_1 \sim k_{-} + k_{+\text{isom}} \\ \lambda_2 \sim \dfrac{k_{-\text{isom}}k_{-}}{k_{-} + k_{+\text{isom}}} \end{cases} \quad \text{(A13)}$$

and eq A11 (the general solution for eq A6) reduces to the following expression:

$$\begin{pmatrix}[\text{M}\cdot\text{L}] \\ [\text{M}\cdot(\text{L})]\end{pmatrix} = C_1\begin{pmatrix}1 \\ \dfrac{-\lambda_1 + k_{-\text{isom}}}{k_{+\text{isom}}}\end{pmatrix}e^{-\lambda_1 t} + C_2\begin{pmatrix}1 \\ \dfrac{-\lambda_2 + k_{-\text{isom}}}{k_{+\text{isom}}}\end{pmatrix}e^{-\lambda_2 t} \quad \text{(A14)}$$

To determine the constants C_1 and C_2, we use the initial partitioning (governed by $k_{+\text{isom}}$ and k_{-}isom) before ligand L dissociation:

$$[\text{M}\cdot\text{L}]_0 = \frac{k_{+\text{isom}}}{k_{+\text{isom}} + k_{-\text{isom}}}, \qquad [\text{M}\cdot(\text{L})]_0 = \frac{k_{-\text{isom}}}{k_{+\text{isom}} + k_{-\text{isom}}} \quad \text{(A15)}$$

At $t = 0$, eq A14 becomes

$$\begin{cases} C_1 + C_2 = \dfrac{k_{+\text{isom}}}{k_{+\text{isom}} + k_{-\text{isom}}} \\ C_1\left(\dfrac{-\lambda_1 + k_{-\text{isom}}}{k_{+\text{isom}}}\right) + C_2\left(\dfrac{-\lambda_2 + k_{-\text{isom}}}{k_{+\text{isom}}}\right) = \dfrac{k_{-\text{isom}}}{k_{+\text{isom}} + k_{-\text{isom}}} \end{cases} \quad \text{(A16)}$$

Solving eq A16 yields C_1 and C_2.

$$\begin{cases} C_1 = \dfrac{-k_{+\text{isom}}\lambda_2}{(\lambda_1 - \lambda_2)(k_{+\text{isom}} + k_{-\text{isom}})} \\ C_2 = \dfrac{k_{+\text{isom}}\lambda_1}{(\lambda_1 - \lambda_2)(k_{+\text{isom}} + k_{-\text{isom}})} \end{cases} \quad \text{(A17)}$$

Therefore, the observed fluorescence signal change is proportional to the change in the concentrations of M·L and M·(L) species:

$$F(t) - F(\infty) \propto [\text{M}\cdot\text{L}] + [\text{M}\cdot(\text{L})] = A_1 e^{-\lambda_1 t} + A_2 e^{-\lambda_2 t} \quad \text{(A18)}$$

where $A_1 + A_2 = 1$ and the amplitude of the fast phase (A_1) is

$$A_1 = C_1 + C_2\left(\frac{-\lambda_1 + k_{-\text{isom}}}{k_{+\text{isom}}}\right) = \frac{k_{-\text{isom}}k_{-} - (k_{+\text{isom}} + k_{-\text{isom}})\lambda_2}{(\lambda_1 - \lambda_2)(k_{+\text{isom}} + k_{-\text{isom}})} \quad \text{(A19)}$$

Under conditions where $k_{-} \gg k_{-\text{isom}}$, the fast phase amplitude (A_1) is determined by the probability of dissociation from the M·(L) state [$k_{-}/(k_{-} + k_{-\text{isom}})$] and the initial population in the M·(L) state [$k_{-\text{isom}}/(k_{+\text{isom}} + k_{-\text{isom}})$] according to

$$A_1 \sim \left(\frac{k_{-\text{isom}}}{k_{+\text{isom}} + k_{-\text{isom}}}\right)\left(\frac{k_{-}}{k_{-} + k_{+\text{isom}}}\right) \quad \text{(A20)}$$

Combination of eq A13 and eq A20 is used to calculate intrinsic rate constants k_{-}, $k_{-\text{isom}}$, and $k_{+\text{isom}}$ from the measured rate constants (λ_1 and λ_2) and the fast phase amplitude (A_1) under conditions where $k_{+} = 0$ and $k_{-} \gg k_{-\text{isom}}$.

Case 2: Ligand (L) Binding to Myosin. Under conditions where $k_+[L] \gg k_{+isom}$, the two rate constants (λ_1 and λ_2) defined by eq A9 reduce to:

$$\begin{cases} \lambda_1 \sim k_- + k_+[L] \\ \lambda_2 \sim k_{-isom} + k_{+isom}\left(\dfrac{k_+[L]}{k_- + k_+[L]}\right) \xrightarrow{\text{if } k_+[L] \gg k_-} k_{-isom} + k_{+isom} \end{cases} \quad \text{(A21)}$$

Therefore, the observed fast rate constant (λ_1) depends linearly on the ligand concentration [L] and the intrinsic rate constants k_+ and k_- can be obtained respectively from the slope and *y*-intercept of the linear fit of the observed fast rate constant versus ligand concentration [L]. For ligand binding measurements, at $t = 0$ [M·L] and [M·(L)] are not populated (i.e. $[M{\cdot}L]_0 = [M{\cdot}(L)]_0 = 0$). Therefore, at $t = 0$, the general solution (eq A11) yields

$$\begin{cases} C_1 + C_2 + \dfrac{k_+[L]k_{+isom}}{k_{-isom}k_- + k_{-isom}k_+[L] + k_{+isom}k_+[L]} = 0 \\ C_1\left(\dfrac{-\lambda_1 + k_{-isom}}{k_{+isom}}\right) + C_2\left(\dfrac{-\lambda_2 + k_{-isom}}{k_{+isom}}\right) + \dfrac{k_+[L]k_{-isom}}{k_{-isom}k_- + k_{-isom}k_+[L] + k_{+isom}k_+[L]} = 0 \end{cases} \quad \text{(A22)}$$

The solutions from eq A22 are

$$\begin{cases} C_1 = \dfrac{k_{+isom}k_+[L]\lambda_2}{(\lambda_1 - \lambda_2)(k_{-isom}k_- + k_{-isom}k_+[L] + k_{+isom}k_+[L])} \\ C_2 = \dfrac{-k_{+isom}k_+[L]\lambda_1}{(\lambda_1 - \lambda_2)(k_{-isom}k_- + k_{-isom}k_+[L] + k_{+isom}k_+[L])} \end{cases} \quad \text{(A23)}$$

Similarly, the observed fluorescence signal change is proportional to the change in concentration of M·L and M·(L) species:

$$F(t) - F(\infty) \propto ([ML] + [M(L)]) - \frac{k_+[L]}{c}(k_{+isom} + k_{-isom}) \propto A_1\, e^{-\lambda_1 t} + A_2\, e^{-\lambda_2 t} \quad \text{(A24)}$$

where c is defined by eq A10, and A_1 and A_2 are the normalized amplitudes ($A_1 + A_2 = 1$):

$$A_1 = C_1\left(\frac{-\lambda_1 + k_{-isom} + k_{+isom}}{k_{+isom}}\right)\Bigg/\left[C_1\left(\frac{-\lambda_1 + k_{-isom} + k_{+isom}}{k_{+isom}}\right) + C_2\left(\frac{-\lambda_2 + k_{-isom} + k_{+isom}}{k_{+isom}}\right)\right] = \frac{\lambda_2(\lambda_1 - k_{-isom} - k_{+isom})}{(\lambda_1 - \lambda_2)(k_{-isom} + k_{+isom})} \sim \frac{k_+[L]}{k_- + k_+[L]} + \left(\frac{k_-}{k_- + k_+[L]}\right)\left(\frac{k_{-isom}}{k_{-isom} + k_{+isom}}\right) \quad \text{(A25)}$$

$$A_2 = C_2\left(\frac{-\lambda_2 + k_{-isom} + k_{+isom}}{k_{+isom}}\right)\Bigg/\left[C_1\left(\frac{-\lambda_1 + k_{-isom} + k_{+isom}}{k_{+isom}}\right) + C_2\left(\frac{-\lambda_2 + k_{-isom} + k_{+isom}}{k_{+isom}}\right)\right] = \frac{\lambda_1(k_{-isom} + k_{+isom} - \lambda_2)}{(\lambda_1 - \lambda_2)(k_{-isom} + k_{+isom})} \sim \left(\frac{k_-}{k_- + k_+[L]}\right)\left(\frac{k_{+isom}}{k_{-isom} + k_{+isom}}\right) \quad \text{(A26)}$$

Under the condition $k_+[L] \gg k_{+isom}$, the normalized fast phase amplitude (A_1) reflects the population binding from M + L to M·(L), ($k_+[L]/(k_- + k_+[L])$), the slow phase is determined by the probability of converting from the weak binding state M(L) to the strong binding state [M·L], ($k_{+isom}/(k_{-isom} + k_{+isom})$), and the remaining population in dissociated (M + L) states, ($k_-/(k_- + k_+[L])$).

A2. Parallel Two-Path Binding Mechanism. The magnesium-dependent two-path parallel mechanism for ligand (L) binding to myosin (M) is defined by the reaction mechanism in Scheme A2, where M·Mg·L represents myosin bound with

Scheme A2

$$\begin{array}{ccc} M\cdot Mg\cdot L & \underset{k_{+1}}{\overset{k_{-1}}{\rightleftharpoons}} & M{+}Mg\cdot L \\ K_{Mg}\uparrow\downarrow\rightleftharpoons Mg & & K'_{Mg}\uparrow\downarrow\rightleftharpoons Mg \\ M\cdot L & \underset{k_{+2}}{\overset{k_{-2}}{\rightleftharpoons}} & M + L \end{array}$$

magnesium (M) and ligand (L), Mg·L is the magnesium−ligand complex, and K_{Mg} and K'_{Mg} are dissociation equilibrium constants for Mg binding. Here, we assume that cation (Mg^{2+}) association and dissociation is very rapid compared to ligand dissociation and occurs within the dead time of the instrument. Therefore, the equilibrium between M·Mg·L and M·L states (equilibrium constant $1/K_{Mg}$) and between Mg·L and L molecules (equilibrium constant $1/K'_{Mg}$) is always maintained (i.e. rapid equilibrium approximation). The differential equations for Scheme A2 under pseudo-first-order conditions are

$$\frac{d}{dt}\{[M{\cdot}Mg{\cdot}L] + [M{\cdot}L]\} = -k_{-1}[M{\cdot}Mg{\cdot}L] - k_{-2}[M{\cdot}L] + k_{+1}[M][Mg{\cdot}L] + k_{+2}[M][L] \quad \text{(A27)}$$

The equilibria between M·Mg·L and M·L states and between Mg·L and L can be expressed as the following relations:

$$[Mg][M{\cdot}L] = K_{Mg}[M{\cdot}Mg{\cdot}L] \quad \text{(A28)}$$

and

$$[Mg][L] = K'_{Mg}[Mg{\cdot}L] \quad \text{(A29)}$$

Combining eqs A28 and A29 yields

$$[M{\cdot}Mg{\cdot}L] + [M{\cdot}L] = [M{\cdot}Mg{\cdot}L] + \left(\frac{K_{Mg}}{[Mg]}\right)[M{\cdot}Mg{\cdot}L] = \left(1 + \frac{K_{Mg}}{[Mg]}\right)[M{\cdot}Mg{\cdot}L] \quad \text{(A30)}$$

which can be rearranged to

$$[\mathrm{M{\cdot}Mg{\cdot}L}] = \left(\frac{[\mathrm{Mg}]}{[\mathrm{Mg}] + K_{\mathrm{Mg}}}\right)([\mathrm{M{\cdot}Mg{\cdot}L}] + [\mathrm{M{\cdot}L}]) \quad \text{(A31)}$$

Similarly, we have

$$[\mathrm{M{\cdot}L}] = \left(\frac{K_{\mathrm{Mg}}}{[\mathrm{Mg}] + K_{\mathrm{Mg}}}\right)([\mathrm{M{\cdot}Mg{\cdot}L}] + [\mathrm{M{\cdot}L}]) \quad \text{(A32)}$$

$$[\mathrm{Mg{\cdot}L}] = \left(\frac{[\mathrm{Mg}]}{[\mathrm{Mg}] + K'_{\mathrm{Mg}}}\right)([\mathrm{Mg{\cdot}L}] + [\mathrm{L}]) \quad \text{(A33)}$$

and

$$[\mathrm{L}] = \left(\frac{K'_{\mathrm{Mg}}}{[\mathrm{Mg}] + K'_{\mathrm{Mg}}}\right)([\mathrm{Mg{\cdot}L}] + [\mathrm{L}]) \quad \text{(A34)}$$

Substituting eqs A31−A34 into eq A27 yields

$$\frac{\mathrm{d}}{\mathrm{d}t}([\mathrm{M{\cdot}Mg{\cdot}L}] + [\mathrm{M{\cdot}L}]) = -\left(\frac{k_{-1}[\mathrm{Mg}] + k_{-2}K_{\mathrm{Mg}}}{[\mathrm{Mg}] + K_{\mathrm{Mg}}}\right)([\mathrm{M{\cdot}Mg{\cdot}L}] + [\mathrm{M{\cdot}L}]) + \left(\frac{k_{+1}[\mathrm{Mg}] + k_{+2}K'_{\mathrm{Mg}}}{[\mathrm{Mg}] + K'_{\mathrm{Mg}}}\right)[\mathrm{M}]([\mathrm{Mg{\cdot}L}] + [\mathrm{L}]) \quad \text{(35)}$$

Therefore, Scheme A2 is equivalent to Scheme A3, where the parentheses are used to indicate a single biochemical state.

Scheme A3

$$(\mathrm{M{\cdot}Mg{\cdot}L} + \mathrm{M{\cdot}L}) \underset{\lambda_+}{\overset{\lambda_-}{\rightleftharpoons}} (\mathrm{M}) + (\mathrm{Mg{\cdot}L} + \mathrm{L})$$

The magnesium concentration-dependent and two-path combined rate constants (λ_- and λ_+) in Scheme A3 are defined by

$$\begin{cases} \lambda_- = \dfrac{k_{-1}[\mathrm{Mg}] + k_{-2}K_{\mathrm{Mg}}}{[\mathrm{Mg}] + K_{\mathrm{Mg}}} \\ \lambda_+ = \dfrac{k_{+1}[\mathrm{Mg}] + k_{+2}K'_{\mathrm{Mg}}}{[\mathrm{Mg}] + K'_{\mathrm{Mg}}} \end{cases} \quad \text{(A36)}$$

REFERENCES

1. Sellers, J. R. (1999) *Myosins*, 2nd ed., Oxford University Press, Oxford.
2. Geeves, M. A., and Holmes, K. C. (1999) Structural mechanism of muscle contraction, *Annu. Rev. Biochem. 68*, 687−728.
3. Goody, R. S., and Hofmann-Goody, W. (2002) Exchange factors, effectors, GAPs and motor proteins: common thermodynamic and kinetic principles for different functions, *Eur. Biophys. J. 31*, 268−74.
4. John, J., Rensland, H., Schlichting, I., Vetter, I., Borasio, G. D., Goody, R. S., and Wittinghofer, A. (1993) Kinetic and structural analysis of the Mg(2+)-binding site of the guanine nucleotide-binding protein p21H-ras, *J. Biol. Chem. 268*, 923−9.
5. Kinosian, H. J., Selden, L. A., Gershman, L. C., and Estes, J. E. (2000) Interdependence of profilin, cation, and nucleotide binding to vertebrate non-muscle actin, *Biochemistry 39*, 13176−88.
6. Cheng, J. Q., Jiang, W., and Hackney, D. D. (1998) Interaction of mant-adenosine nucleotides and magnesium with kinesin, *Biochemistry 37*, 5288−95.
7. De La Cruz, E. M., Wells, A. L., Rosenfeld, S. S., Ostap, E. M., and Sweeney, H. L. (1999) The kinetic mechanism of myosin V, *Proc. Natl. Acad. Sci. U.S.A. 96*, 13726−31.
8. Hiratsuka, T. (1983) New ribose-modified fluorescent analogs of adenine and guanine nucleotides available as substrates for various enzymes, *Biochim. Biophys. Acta 742*, 496−508.
9. De La Cruz, E. M., Wells, A. L., Sweeney, H. L., and Ostap, E. M. (2000) Actin and light chain isoform dependence of myosin V kinetics, *Biochemistry 39*, 14196−202.
10. Wilson, J. E., and Chin, A. (1991) Chelation of divalent cations by ATP, studied by titration calorimetry, *Anal. Biochem. 193*, 16−9.
11. Wiseman, T., Williston, S., Brandts, J. F., and Lin, L. N. (1989) Rapid measurement of binding constants and heats of binding using a new titration calorimeter, *Anal. Biochem. 179*, 131−7.
12. Robblee, J. P., Henn, A., Hannemann, D. E., and De La Cruz, E. M. (2005) Thermodynamics of Nucleotide Binding to Actomyosin V and VI: A Positive Heat Capacity Change Accompanies Strong ADP Binding, *Biochemistry*, submitted.
13. Trybus, K. M., Krementsova, E., and Freyzon, Y. (1999) Kinetic characterization of a monomeric unconventional myosin V construct, *J. Biol. Chem. 274*, 27448−56.
14. Wang, F., Chen, L., Arcucci, O., Harvey, E. V., Bowers, B., Xu, Y., Hammer, J. A., 3rd, and Sellers, J. R. (2000) Effect of ADP and ionic strength on the kinetic and motile properties of recombinant mouse myosin V, *J. Biol. Chem. 275*, 4329−35.
15. Geeves, M. A., and Conibear, P. B. (1995) The role of three-state docking of myosin S1 with actin in force generation, *Biophys. J. 68*, 194S−199S; discussion 199S−201S.
16. Geeves, M. A., Goody, R. S., and Gutfreund, H. (1984) Kinetics of acto-S1 interaction as a guide to a model for the crossbridge cycle, *J. Muscle Res. Cell Motil. 5*, 351−61.
17. Cremo, C. R., and Geeves, M. A. (1998) Interaction of actin and ADP with the head domain of smooth muscle myosin: implications for strain-dependent ADP release in smooth muscle, *Biochemistry 37*, 1969−78.
18. Rosenfeld, S. S., Houdusse, A., and Sweeney, H. L. (2005) Magnesium regulates ADP dissociation from myosin V, *J. Biol. Chem. 280*, 6072−9.
19. Rosenfeld, S. S., Xing, J., Whitaker, M., Cheung, H. C., Brown, F., Wells, A., Milligan, R. A., and Sweeney, H. L. (2000) Kinetic and spectroscopic evidence for three actomyosin:ADP states in smooth muscle, *J. Biol. Chem. 275*, 25418−26.
20. Uemura, S., Higuchi, H., Olivares, A. O., De La Cruz, E. M., and Ishiwata, S. (2004) Mechanochemical coupling of two substeps in a single myosin V motor, *Nat. Struct. Mol. Biol. 11*, 877−83.
21. Mehta, A. D., Rock, R. S., Rief, M., Spudich, J. A., Mooseker, M. S., and Cheney, R. E. (1999) Myosin-V is a processive actin-based motor, *Nature 400*, 590−3.
22. Nyitrai, M., and Geeves, M. A. (2004) Adenosine diphosphate and strain sensitivity in myosin motors, *Philos. Trans. R. Soc. London, Ser. B 359*, 1867−77.
23. Conibear, P. B. (1999) Kinetic studies on the effects of ADP and ionic strength on the interaction between myosin subfragment-1 and actin: implications for load-sensitivity and regulation of the crossbridge cycle, *J. Muscle Res. Cell Motil. 20*, 727−42.
24. Baker, J. E., Krementsova, E. B., Kennedy, G. G., Armstrong, A., Trybus, K. M., and Warshaw, D. M. (2004) Myosin V processivity: multiple kinetic pathways for head-to-head coordination, *Proc. Natl. Acad. Sci. U.S.A. 101*, 5542−6.
25. Coureux, P. D., Wells, A. L., Menetrey, J., Yengo, C. M., Morris, C. A., Sweeney, H. L., and Houdusse, A. (2003) A structural state of the myosin V motor without bound nucleotide, *Nature 425*, 419−23.
26. Coureux, P. D., Sweeney, H. L., and Houdusse, A. (2004) Three myosin V structures delineate essential features of chemo-mechanical transduction, *EMBO J. 23*, 4527−37.
27. Jontes, J. D., Milligan, R. A., Pollard, T. D., and Ostap, E. M. (1997) Kinetic characterization of brush border myosin-I ATPase, *Proc. Natl. Acad. Sci. U.S.A. 94*, 14332−7.
28. Kovacs, M., Wang, F., and Sellers, J. R. (2005) Mechanism of action of myosin X, a membrane-associated molecular motor, *J. Biol. Chem. 280*, 15071−83.
29. Morita, F. (1977) Temperature induced analog reaction of adenylyl imidodiphosphate to an intermediate step of heavy meromyosin adenosine triphosphatase, *J. Biochem. (Tokyo) 81*, 313−20.
30. Bechet, J. J., Breda, C., Guinand, S., Hill, M., and d'Albis, A. (1979) Magnesium ion dependent adenosine triphosphatase activity

of heavy meromyosin as a function of temperature between +20 and −15 degrees C, *Biochemistry 18*, 4080−9.
31. Sleep, J. A., and Hutton, R. L. (1980) Exchange between inorganic phosphate and adenosine 5′-triphosphate in the medium by actomyosin subfragment 1, *Biochemistry 19*, 1276−83.
32. Shriver, J. W., and Sykes, B. D. (1981) Energetics and kinetics of interconversion of two myosin subfragment-1.adenosine 5′-diphosphate complexes as viewed by phosphorus-31 nuclear magnetic resonance, *Biochemistry 20*, 6357−62.
33. Shriver, J. W., and Sykes, B. D. (1981) Phosphorus-31 nuclear magnetic resonance evidence for two conformations of myosin subfragment-1.nucleotide complexes, *Biochemistry 20*, 2004−12.
34. Aguirre, R., Lin, S. H., Gonsoulin, F., Wang, C. K., and Cheung, H. C. (1989) Characterization of the ethenoadenosine diphosphate binding site of myosin subfragment 1. Energetics of the equilibrium between two states of nucleotide.S1 and vanadate-induced global conformation changes detected by energy transfer, *Biochemistry 28*, 799−807.
35. Trybus, K. M., and Taylor, E. W. (1982) Transient kinetics of adenosine 5′-diphosphate and adenosine 5′-(beta, gamma-imidotriphosphate) binding to subfragment 1 and actosubfragment 1, *Biochemistry 21*, 1284−94.
36. Trybus, K. M., and Taylor, E. W. (1980) Kinetic studies of the cooperative binding of subfragment 1 to regulated actin, *Proc. Natl. Acad. Sci. U.S.A. 77*, 7209−13.
37. Garland, F., Gonsoulin, F., and Cheung, H. C. (1988) The MgADP-induced decrease of the SH1-SH2 fluorescence resonance energy transfer distance of myosin subfragment 1 occurs in two kinetic steps, *J. Biol. Chem. 263*, 11621−3.
38. Coates, J. H., Criddle, A. H., and Geeves, M. A. (1985) Pressure-relaxation studies of pyrene-labelled actin and myosin subfragment 1 from rabbit skeletal muscle. Evidence for two states of acto-subfragment 1, *Biochem. J. 232*, 351−6.
39. Geeves, M. A. (1989) Dynamic interaction between actin and myosin subfragment 1 in the presence of ADP, *Biochemistry 28*, 5864−71.
40. Woodward, S. K., Eccleston, J. F., and Geeves, M. A. (1991) Kinetics of the interaction of 2′(3′)-O-(N-methylanthraniloyl)-ATP with myosin subfragment 1 and actomyosin subfragment 1: characterization of two acto-S1-ADP complexes, *Biochemistry 30*, 422−30.
41. Fisher, A. J., Smith, C. A., Thoden, J. B., Smith, R., Sutoh, K., Holden, H. M., and Rayment, I. (1995) X-ray structures of the myosin motor domain of Dictyostelium discoideum complexed with MgADP.BeFx and MgADP.AlF4, *Biochemistry 34*, 8960−72.
42. Dominguez, R., Freyzon, Y., Trybus, K. M., and Cohen, C. (1998) Crystal structure of a vertebrate smooth muscle myosin motor domain and its complex with the essential light chain: visualization of the pre-power stroke state, *Cell 94*, 559−71.
43. Whittaker, M., Wilson-Kubalek, E. M., Smith, J. E., Faust, L., Milligan, R. A., and Sweeney, H. L. (1995) A 35-Å movement of smooth muscle myosin on ADP release, *Nature 378*, 748−51.
44. Taylor, E. W. (1991) Kinetic studies on the association and dissociation of myosin subfragment 1 and actin, *J. Biol. Chem. 266*, 294−302.
45. Walker, M., Zhang, X. Z., Jiang, W., Trinick, J., and White, H. D. (1999) Observation of transient disorder during myosin subfragment-1 binding to actin by stopped-flow fluorescence and millisecond time resolution electron cryomicroscopy: evidence that the start of the crossbridge power stroke in muscle has variable geometry, *Proc. Natl. Acad. Sci. U.S.A. 96*, 465−70.
46. Bagshaw, C. R., and Reed, G. H. (1976) Investigations of equilibrium complexes of myoxin subfragment 1 with the manganous ion and adenosine diphosphate using magnetic resonance techniques, *J. Biol. Chem. 251*, 1975−83.
47. Mandelkow, E. M., and Mandelkow, E. (1973) Fluorimetric studies on the influence of metal ions and chelators on the interaction between myosin and ATP, *FEBS Lett. 33*, 161−6.
48. Bagshaw, C. R., and Trentham, D. R. (1974) The characterization of myosin-product complexes and of product-release steps during the magnesium ion-dependent adenosine triphosphatase reaction, *Biochem. J. 141*, 331−49.

BI0473509